ROLES OF REV1 POLYMERASE AND FANCJ HELICASE IN G-QUADRUPLEX UNWINDING AND DNA DAMAGE TOLERANCE

by

ALYSSA PAUL

A thesis submitted in partial fulfillment of the
requirements for the degree of

MASTER OF SCIENCE IN BIOLOGY

2026

Oakland University
Rochester, Michigan

Thesis Advisory Committee:

Colin G. Wu, Ph.D., Chair
Adam Avery, Ph.D.
Luis G. Villa-Diaz, Ph.D.

To my mother and father

ACKNOWLEDGMENTS

I want to express my deepest gratitude to Dr. Colin Wu who has mentored me throughout my undergraduate and graduate studies. I am incredibly grateful for the opportunities he has presented to work in his lab and pursue a master's degree under his direction. His instruction and guidance have been invaluable in my education.

To Dr. Avery and Dr. Villa-Diaz, thank you so much for your support and willingness to serve on my thesis advisory committee. Dr. Avery, your input into my education as both a professor and mentor has been greatly appreciated.

I would like to thank my family and friends who have provided unwavering love and support. To my parents, you are both an inspiration and huge encouragement. I cannot thank you enough for everything you do.

To all of the Wu lab members, thank you for your support and for making the lab an enjoyable place to come each day. I want to extend thanks to Dr. Kaitlin Lowran for all of her help and guidance and to Jennifer Jaster for assisting with experiments.

Above all, I want to praise God for all that He has done and allows me to do. Everything I am and do is fully dedicated to the Lord.

ALYSSA NOREEN LESLEY PAUL

ABSTRACT

ROLES OF REV1 POLYMERASE AND FANCJ HELICASE IN G-QUADRUPLEX UNWINDING AND DNA DAMAGE TOLERANCE

by

ALYSSA PAUL

Adviser: Colin G. Wu, Ph.D.

DNA damage repair pathways are essential to continue replication past DNA lesions and secondary structures such as G-quadruplexes (G4s). Unresolved G4s pose a threat to genomic stability due to their formation in common oncogenic promoters and telomeres. The DNA damage repair proteins REV1 polymerase and FANCJ helicase are capable of unfolding G4s to allow their replication. In this study, we examined the G4 unfolding efficiencies of REV1 and FANCJ for parallel $(GGGT)_4$ and hybrid $(TTAGGG)_4$ sequences with and without oxidative damage (8oxoG4) using BMVC fluorescence assays and hemin colorimetric assays. We suspected that REV1 and FANCJ would demonstrate a preference for different G4 conformations, and that 8oxoG4s would be more efficiently unfolded compared to undamaged sequences. Additionally, we investigated the effects of the DNA damage inducers menadione and bleomycin on HEK293T cells with FANCJ upregulation. We expected that increasing treatment concentrations would induce increasing DNA damage and that FANCJ upregulation would suppress this damage. The unfolding data revealed that REV1 preferentially resolved $(TTAGGG)_4$ structures compared to $(GGGT)_4$ and that REV1 unwound these

structures with a higher efficiency compared to FANCJ. Conversely, FANCJ preferentially unfolded $(GGGT)_4$ structures, and did so more efficiently than REV1. Both proteins were capable of unfolding 8oxoG4s, with oxidative damage impacting unfolding differently for each G4 sequence and protein pair. REV1 and FANCJ were also capable of unfolding G4s with and without ATP. Damage induction results showed that 0.001-10 μM menadione triggered DNA damage response pathways to suppress damage and did not yield a measurable increase in damage. The transfection of FANCJ caused a similar response in menadione-treated cells, with decreased DNA damage compared to untransfected cells. Bleomycin-treated cells did demonstrate increasing DNA damage, and FANCJ upregulation suppressed damage at higher treatment concentrations compared to low-efficiency transfection or untransfected cells. Overall, these results show that REV1 and FANCJ binding is sufficient to unfold G4s and suggests a model in which FANCJ targets and unfolds hybrid G4s then recruits REV1 to continue DNA replication, while REV1 unfolds parallel G4 structures before continuing replication or recruiting other TLS pols. Additionally, the upregulation of FANCJ may improve the damage suppression response for cells exposed to bleomycin, suggesting that protein upregulation in non-cancerous cells could have a protective effect against DNA damage inducers.

TABLE OF CONTENTS

TABLE OF CONTENTS—Continued

TABLE OF CONTENTS—Continued

LIST OF TABLES

LIST OF FIGURES

LIST OF ABBREVIATIONS

DNA	Deoxyribonucleic acid
pol	Polymerase
HR	Homologous recombination
TLS	Translesion synthesis
PCNA	Proliferating cell nuclear antigen
PIP	PCNA-interacting-peptide
CTD	C-terminal domain
8oxoG	8-oxoguanine
G4	G-quadruplex
ssDNA	Single-stranded DNA
FA	Fanconi Anemia
FANC	Fanconi Anemia complementation group
FAAP	Fanconi Anemia associated protein
ICL	Interstrand crosslink
D2-I	FANCD2-FANCI complex
BRCT	BRCA1 C-terminal domain
dsDNA	Double-stranded DNA
UBM	Ubiquitin binding motif
siRNA	silencing RNA
BMVC	3,6-bis(1-Methyl-4-vinylpyridinium) carbazole diiodide
PMSF	phenylmethylsulfonyl fluoride

HF	HighFive
ATP	Adenosine triphosphate
HEK	Human embryonic kidney
PEI	Polyethylenimine
FBS	Fetal bovine serum
ROS	Reactive oxygen species
MQ	Ultra-pure type I water

CHAPTER ONE

INTRODUCTION

1.0 DNA Damage Response Pathways

Deoxyribonucleic acid (DNA) damage response pathways are the collection of vital cellular processes which utilize proteins capable of targeting and repairing DNA damage to allow the smooth progression of DNA replication and mitigate mutagenesis. In general, there are two major damage repair responses. One allows for the quick continuation past lesions through an error-prone bypass via low-fidelity polymerases (pols) or fork repriming [1, 2]. The second utilizes homologous recombination (HR) or fork reversal to repair the lesion before continuing replication [1, 2]. Both general pathways maintain fork progression, allowing DNA replication and cell survival. When these pathways are inhibited, damage accumulation can lead to disease or cancer growth and fork collapse can cause cell death [1, 2]. As such, understanding damage suppression pathways, their connections to one another, and their mechanism of DNA repair are vital in the search for mechanistic targets to combat diseases related to genomic instability.

1.0.1 Translesion Synthesis Repair Pathway and REV1

The translesion synthesis (TLS) repair pathway consists of low-fidelity polymerases that collectively promote DNA stability by enabling replication to proceed past DNA lesions [1, 2, 3]. While the error-prone TLS pols pose an added risk of mutagenesis from incorrect base insertion, the pathway prioritizes cell survival via the efficient bypass of lethal lesions [1, 2, 4].

The TLS pathway is triggered by the monoubiquitination of the DNA sliding clamp and replication processivity factor proliferating cell nuclear antigen (PCNA) after it has located a stalled fork [1, 2]. Monoubiquitinated PCNA acts as a scaffold, recruiting TLS pols to the lesion site by interacting with a PCNA-interacting-peptide (PIP) motif within each pol [1, 2]. Once assembled, the pols can replicate past the lesion and replication can progress normally.

The largest family of TLS pols is the Y-family, which includes REV1, pol eta, pol iota, and pol kappa [1, 2]. While all TLS pols are error-prone, REV1 is unique due to its deviation from Watson-Crick pairing altogether [3, 5]. Most polymerases use the four templating DNA bases to direct the insertion of the correct base pair, each with similar efficiency. REV1, however, uses a protein-template mechanism to bind preferentially to guanine and direct the almost exclusive insertion of cytosine [3, 5]. The catalytic core of REV1 is responsible for the preferential pairing of the pol to a templating guanine [6, 7]. When a templating guanine reaches the active site of REV1, it is evicted by Leu325 and positioned in a hydrophobic pocket formed by the core's G-loop domain [6, 7, 8]. The pocket preferentially bonds to the N7 and O^6 atoms of guanine and ensures its specificity, as the other bases are not able to participate in the same pattern of hydrogen bonding [6, 9]. Thus, REV1 preferentially binds to guanine rich sequences during DNA repair.

The protein-template mechanism of REV1 does not apply solely to the templating base. While REV1 is capable of inserting guanine, thymine, and adenine across from the templating strand, the catalytic efficiency of insertion decreases drastically from that of cytosine [6, 7]. Instead of using the templating base to direct in a complementary base, Arg324 of REV1 directly binds dCTP before nucleotide insertion [9]. This means that

REV1 is capable of inserting a cytosine across from any base as well as abasic sites [9]. As such, while REV1 has a 25-fold higher binding efficiency for a templating base compared to abasic sites, REV1 incorporates dCTP across from abasic sites without a decline in catalytic efficiency [9]. Overall, the protein-mediated specificity of REV1 for a templating guanine and dCTP may be essential in replication processivity past DNA lesions in guanine rich regions of DNA.

While the REV1 polymerase is capable of catalytic activity, this is not considered its primary role within the TLS pathway. Instead, REV1 plays a vital role as a scaffold protein, binding other TLS pols via its C-terminal domain (CTD) [5]. REV1 interacts with pol eta, pol iota, pol kappa, and the REV7 subunit of pol zeta, helping the proteins localize to the diverse types of DNA damage each pol is specialized to repair [6, 10]. These include UV lesions, oxidatively damaged guanine (8oxoG), N^2-guanine adducts, aldehyde-induced interstrand cross links, and O^6-alkylguanine [6, 11, 12, 13, 14]. REV1 is also involved in the unfolding and replication of a complex DNA secondary structure known as a G-quadruplex (G4) through direct binding and recruitment of additional pols [5].

Overall, the TLS pathway effectively maintains fork progression past lesions, however in an error-prone manner. While the loss of function of TLS proteins results in fork collapse and cell death, the upregulation of these proteins is a common finding in cancer cells [15, 16]. The upregulation of DNA damage repair proteins likely contributes to cancer adaptability and evasion of chemotherapeutic drugs [16]. TLS pols have been observed to aid in cancer cell survival through replication gap suppression by repairing single-stranded DNA (ssDNA) breaks that occur during replication [16]. Because of this,

suppression of the TLS pathway through small molecule inhibition of its pols is being investigated as a potential cancer therapy [4, 16]. Different pols have been observed to be upregulated depending on the cancer type [4, 16]. By investigating the TLS pols and bringing a better understanding of their mechanisms of action, new drugs can be developed for individualized treatments which target proteins based on those upregulated in a specific cancer type.

1.0.2 Fanconi Anemia Repair Pathway and FANCJ

The Fanconi Anemia (FA) repair pathway consists of several FANC (FA complementation group) proteins and additional associated proteins (FAAP) involved in interstrand crosslink (ICL) removal and HR-directed repair of lesions [17]. This pathway allows the progression of DNA replication at ICL sites by locating, stabilizing, and repairing the lesions using a homologous DNA template [1, 2]. Currently mutations within 23 FA genes have been identified to cause the disease by which the pathway is named [17]. FA is characterized by genetic instability due to hindered DNA repair mechanisms, especially in the hematopoietic system [17, 18, 19]. In FA diseased cells, the p53 tumor suppressor gene is abnormally upregulated in response to DNA damage and signals a p21 dependent halt in cell division and subsequent apoptosis of the cell [19]. The increase of cell cycle arrest in susceptible hematopoietic stem cells leads to bone marrow failure and an overall deficiency of white and red blood cells and platelets [17, 19]. FA patients also have a heightened risk of cancer development due to the inhibition of DNA repair mechanisms and the subsequent accumulation of mutations [17, 19]. Due to its strong link to cancer development, the FA pathway presents potential therapeutic targets not just to relieve FA symptoms, but for cancer therapies as well [2].

In order for scientists to develop new treatments for both FA and cancer it is essential to investigate and understand the components of the FA repair pathway, as well as their connections to other repair pathways.

The FA pathway is initiated through a cascade of interactions in response to DNA damage. The key initiating step of FA repair is the monoubiquitination of the FANCD2-FANCI complex (D2-I) by the FA core complex [17, 20, 21, 22]. The core complex is made of a set of eight essential FA proteins (FANCA, FANCB, FANCC, FANCE, FANCF, FANCG, FANCL, FANCM) and two FA associated proteins (FAAP20, FAAP100) [17]. Mutations in any of the eight core proteins cause FA disease [17]. The catalytic component of the core is FANCL, an E3 ubiquitin ligase, and is responsible for the monoubiquitination of the D2-I complex [17, 23]. This complex acts as a sliding-clamp that binds DNA and is stalled at lesions [17, 20, 21, 22]. Once monoubiquitinated, the D2-I complex is activated and helps localize other FA proteins to the site of damage [17, 20, 21]. The damage is then repaired by FA proteins through HR and the pathway is turned off by the deubiquitination of the D2-I clamp [20, 21].

A notable protein within the FA pathway is the 5'-3' FANCJ helicase. This is the only known helicase within the FA pathway and is essential in FA directed HR and ICL repair [24, 25]. FANCJ was originally discovered by its interaction with the C-terminus of BRCA1 (BRCT) and found to be necessary for double-stranded DNA (dsDNA) break repair facilitated by BRCA1 [26]. Mutations within FANCJ cause FA disease, increased mutagenesis, and are a susceptibility marker for breast and ovarian cancer [27]. Within the FA pathway, FANCJ is suspected to act downstream or parallel to the monoubiquitination of the D2-I complex [24]. FANCJ knockout models exhibit normal

FANCD2 monoubiquitination, however, studies have found that FANCJ may be necessary to localize the monoubiquitinated clamp to DNA damage sites [28]. Additionally, the termination of the FA repair pathway by the deubiquitination of the D2-I complex may serve to halt unwinding activity by FANCJ through an increase in the binding affinity of FANCD2 for FANCJ, which sequesters the helicase away from DNA [29]. FANCJ unwinds duplex DNA in an ATP dependent manner, via its conserved helicase core domain which contains an Fe-S cluster that is required for the helicase's function [30]. In addition to unwinding D-loops which form early in HR, FANCJ exhibits an important role in G4 recognition and unwinding [31]. The essential role and diverse function of FANCJ as a DNA repair helicase both within and outside of the FA pathway makes this protein a notable target to investigate.

Overall, the FA repair pathway is capable of repairing DNA in a manner less error-prone than the TLS pathway due to the utilization of HR. While this type of repair reduces mutagenesis in healthy cells, the overexpression of FA proteins in cancer cells functions similarly to TLS pols to promote cancer vitality [32]. Through a similar process of damage suppression, the overactivity of FA proteins in cancer cells can confer drug resistance through the repair of chemotherapy induced damage. Like TLS pols, the ability of FA proteins to be both inhibitive and supportive of cancer cell proliferation makes these proteins necessary to understand as scientists progress in cancer research.

1.0.3 Interaction Between TLS and FA Repair Pathways

The current understanding of individual DNA damage repair pathways forms a vital scaffold to build upon as the interactions between pathways are investigated. While the TLS and FA repair pathways target different types of damage with independent

mechanisms, several proteins have been found to interact between these two pathways. The FA pathway's D2-I complex recruits FA proteins to damage sites, but recent evidence shows it can recruit TLS pols as well [21, 33]. Monoubiquitinated FANCD2 has been shown to interact with the ubiquitin binding motif (UBM) within the CTD of the TLS pol REV1 [33]. This interaction helps to localize REV1 to dsDNA breaks, and depletion of either FANCD2 or FANCD1 (BRCA2) reduces the localization of REV1 at UV induced DNA lesions and increases damage accumulation [33]. In both the TLS and FA pathways, REV1 serves as a scaffold for REV7 (FANCV), helping recruit this pol and the associated pol zeta to damage sites to continue replication [21, 33, 34]. The REV1-CTD is also capable of interacting with a PIP-like domain on FANCJ [5, 35, 36].

The interaction between REV1 and FANCJ is of particular interest due to evidence that both proteins independently play roles in the promotion of genomic stability at G4 sites [5, 35, 36, 37, 38]. The maintenance of non-canonical G4 folds is a mechanism outside of the typical TLS or FA repair pathways. Understanding the role these proteins play in G4 maintenance will help to uncover the interactions between the TLS and FA pathways.

1.1 G-Quadruplexes

G4s are secondary structures of DNA or RNA that can form in guanine rich regions. Tandem runs of guanine can participate in Hoogsteen hydrogen bonding to form a planar G-tetrad stabilized by a central monovalent cation, typically Na^+ or K^+ [39]. When two or more of these tetrads stack together, the resulting structure is a G4 (Figure 1.1) [39].

There are approximately 10,000 confirmed G4 forming sequences within the human genome under physiological conditions [40]. These sequences follow a general template sequence $G_{\geq 2}N_{1\text{-}7}G_{\geq 2}N_{1\text{-}7}G_{\geq 2}N_{1\text{-}7}G_{\geq 2}N_{1\text{-}7}$, where G is a run of two or more guanines and N is any other base forming a one to seven nucleotide loop [39]. These structures are able to form intramolecularly into parallel, anti-parallel, and hybrid conformations depending on DNA directionality (Figure 1.1) [35, 41, 42]. Each of these G4 forming sequences have the potential to threaten genomic stability due to their ability to stall replication forks in promoter regions and telomeres [40, 43]. Additionally, with the lowest reduction-oxidation potential of the nucleic acid bases, the high density of guanines in G4s makes these structures susceptible to oxidative stress and damage accumulation, leading to the formation of mutagenic 8oxoG4s (8-oxoguanine) [44, 45]. The type of central cation, G4 conformation, loop length, and the presence and position of oxidative damage, all contribute to changes in G4 stability and may impact G4 unfolding [35, 41, 42].

When G4 unfolding is hindered, mutations accumulate downstream G4 sites, contributing to cancer development or preventing replication altogether and halting cell proliferation [39]. G4 initiated mutagenesis can contribute to cancer growth depending on G4 position by causing mutations that switch oncogenic promoters on or by turning off tumor suppressor genes [46]. The stabilization of G4s by G4 ligands have demonstrated promising anticancer capacities by stalling replication and leading to cancer cell death [46, 47, 48, 49]. In order to continue the search for antitumor agents targeting G4s, it is pertinent to understand the normal mechanism behind G4 unfolding and replication.

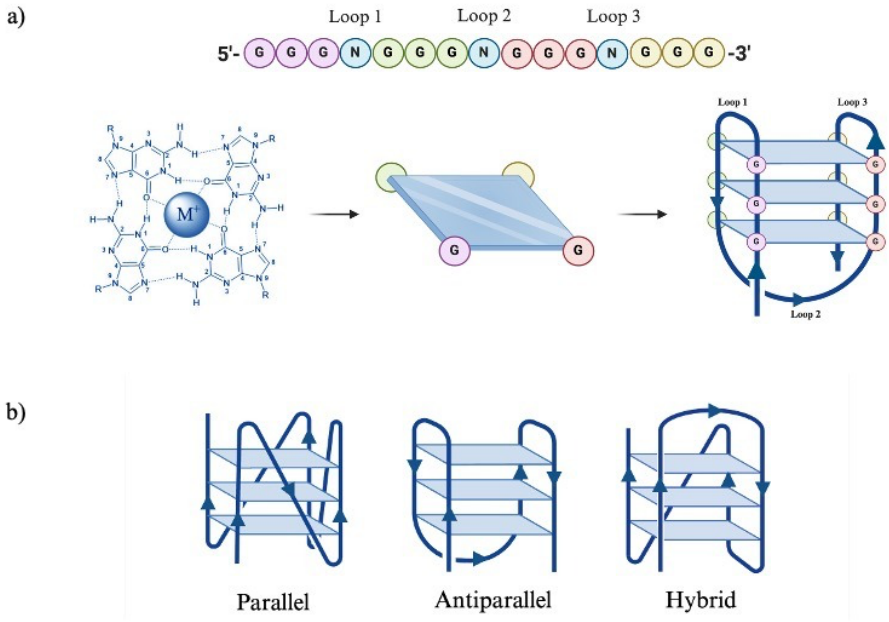

Figure 1.1: G4 formation and possible conformations: a) The formation of a G4 from a DNA sequence containing four tandem repeats of guanine runs separated by N number of nucleotides. The guanine runs hydrogen bond to form a planar tetrad stabilized by a monovalent cation. Multiple tetrads stack to form the G4. b) Parallel, antiparallel, and hybrid G4 folding conformations are depicted. The conformation is determined by the orientation of neighboring guanine runs. Parallel G4s are all oriented in the same direction, parallel G4s alternate direction, and hybrid G4s contain a mixture of both orientations. This figure is adapted from *Mechanisms of G-Quadruplex Recognition and Unfolding by the FANCJ Helicase and REV1 Polymerase* [50].

1.1.1 TLS Repair Pathway and G4s

G4s left unfolded will stall a replication fork by blocking the main replicative pols alpha, delta, and epsilon [5]. To bypass these complex folds during DNA replication,

proteins capable of unfolding G4s and continuing replication must be recruited to the site.

The TLS repair pathway has been found to help maintain genomic stability at G4 sites through the direct interaction between TLS pols and G4s. Specifically, TLS pols eta and kappa have demonstrated an ability to promote genomic stability around G4 sites [51, 52, 53]. One study found that the downregulation of these pols sensitized cells to G4 stabilization via the G4 ligand telomestatin and led to dsDNA break accumulation at G4 sites and a subsequent decrease in cell proliferation [51]. While the mechanism of G4 maintenance by these pols is not well understood, pol kappa does exhibit a 5.7-fold higher affinity for G4 DNA over non-G4 sequences [52]. As such, it is likely that direct binding of pol kappa promotes G4 unfolding and allows replication to proceed either by pol kappa or pol eta [52].

REV1 also plays a role in G4 maintenance by preferentially binding and unfolding G4s via an insert-2 motif within the finger domains of its catalytic core [37, 38]. REV1 preferentially binds to G4 DNA with up to a 15-fold higher affinity compared to non-G4 forming sequences [37, 38]. The binding of REV1 relaxes the G4 and enables either REV1 or other TLS pols to continue replication across the sequence. The highly specific REV1 mediated addition of cytosine may be a vital step to avoid mutations during the bypass of guanine rich G4 sequences. Previous studies have shown that REV1 deficient cells demonstrate genomic instability in post-replication gaps and downstream G4s in avian cell lines [54, 55]. Supporting these findings, a recent study found that downregulating REV1 through siRNA inhibition or small molecule inhibition with a

REV1 ligand in HEK293 cells lead to instability and mutability in trinucleotide repeats [56].

The TLS repair pathway pols seem to be a key component in the maintenance of genomic stability at G4s. The G4 structure, however, is not targeted by TLS pols alone. Instead, it is likely that the TLS and FA pathways work together to unfold and replicate G4s.

1.1.2 FA Repair Pathway and G4s

The FA proteins have not exhibited as extensive a role in G4 maintenance as the TLS pols, but FANCJ has been found to interact with REV1 in damage repair and G4 regulation [5, 35, 36]. Additionally, FANCJ helicase is unique among its pathway proteins due to its ability to directly bind and unfold G4s via an AKKQ motif [35]. Studies have found that FANCJ maintains genomic stability at G4 sites through two pathways, involving either REV1 or the helicases WRN and BLM [36]. The downregulation of FANCJ results in post-replication deletions at G4 sites, resulting in increased mutagenesis and cell mortality [36, 55]. Because of this, investigating the interaction between REV1 and FANCJ is important to expand the current understanding of G4 localization, unwinding, and replication. As more is known about DNA repair proteins and their involvement with the mutagenic G4 structure, targeted cancer treatments can be advanced.

1.2 Thesis Research

Each year in the US, approximately two million cases of cancer are diagnosed and around 600,000 cancer patients die of the disease [48]. While some cancers can be managed with available treatment options, not all respond well. Because of this, it is

essential to continue the search for new cancer therapies and expand our knowledge of the DNA repair mechanisms that suppress mutagenesis and cancer formation.

In recent years, G4s have gained interest in the landscape of cancer research. Studies have found an increase in G4 formation during the S-phase of the cell cycle of cancerous cells compared to normal cells [48, 58]. While this finding does not distinguish between increased G4 formation as the cause of cancer versus a product of cancer, G4s have demonstrated mutagenic properties. Mutations around G4s located in oncogenic promoters can be a switch to activate promoters and induce cancerous cell division [47, 48]. G4s have been localized to common cancer oncogenes such as KRAS, MYC, KIT, VEGF, VEGF-R, mTOR, and HIF1a [47]. The association between G4s and cancer is so strong, that these structures are being investigated as a potential biomarker for certain cancer types [58]. Additionally, scientists have begun targeting G4s with stabilizing ligands as a potential cancer therapy [47, 48, 49].

The replication of telomeric G4s is vital for cancer cell survival. In rapidly replicating cancer cells, telomeric shortening poses a serious threat. In cancer cells, the enzyme responsible for telomeric elongation - telomerase - is often upregulated [59]. G4 ligands stabilizing telomeric sequences demonstrate antitumorigenic properties through the inhibition of telomeric elongation [46, 47, 48]. By blocking telomerase, the subsequent telomeric shortening results in less robust cancer cell proliferation [46, 47, 48]. While G4 ligands were originally assumed to act primarily through telomerase inhibition, this mechanism would require multiple rounds of division before leading to cell death. This could be an effective long term antitumor strategy, however G4 ligands such as RHPS4 have demonstrated a faster antitumoral effect [47, 60]. The ligand was

discovered to inhibit cancer proliferation through the promotion of telomere dysfunction, topological stress, and DNA damage accumulation [47, 60]. Other G4 ligands have been found to inhibit cell growth through modulation of gene expression within cancer regulatory regions [47]. The ligand TMPyP4 demonstrates anticancer properties by stabilizing a G4 within the promoter region of the c-Myc gene, decreasing expression [47, 61]. The common formation of G4s within promoters of cancer oncogenes makes the targeting of these structures potentially profitable in reducing oncogenic expression.

A challenge of G4-ligand based therapy lies within their selectivity for G4s [47, 60]. As of 2025 there were over 4,800 G4 ligands recorded in the G4 Ligand Database, which was established in 2013 [49]. While many ligands demonstrate excellent affinity for G4s *in vitro* or in cell-based assays, off-target effects have been a common barrier thus far in preclinical research [47, 60]. Despite this, scientists are still searching for ways to target the G4 structure in a therapeutic approach.

DNA damage repair proteins also present a potential target in anticancer research. These proteins may be upregulated in rapidly dividing cancer cells, suppressing mutagenesis that would lead to apoptosis [2, 4, 32]. REV1 has been found to be upregulated in lung cancer tissue compared to healthy lung tissue [62]. The contribution of REV1 in cancer growth was investigated using silencing RNA (siRNA) to downregulate the protein [62]. The REV1 inhibitor JH-RE-06 was also used to decrease REV1 function by promoting post-translational nonfunctional dimer formation [62]. Compared to untreated cancer cells, REV1 depleted cells from either siRNA or JH-RE-06 treatment demonstrated limited replication and higher mortality rates when treated with the chemotherapeutic drug cisplatin [62]. This finding suggests that targeting DNA repair

pathway proteins may provide novel therapeutic approaches by dampening the viability of aggressive cancers and making current treatment options more effective.

1.2.1 Research Hypotheses

In our lab, we have been investigating REV1 polymerase and FANCJ helicase. Specifically, we have been examining their roles in G4 unfolding and the effects of their upregulation on DNA damage suppression. By investigating the role of these proteins in G4 unfolding we can gain a better understanding of the mechanisms behind the maintenance of genomic stability at G4 sites. Additionally, by determining the effect of upregulation in healthy cells exposed to damage inducers, we can examine the potential protective effect of these proteins in non-cancer cells. As more is revealed about the healthy cell maintenance at G4 and damage sites, this information can be used to advance the search for targeted cancer therapies using G4s and DNA damage repair proteins.

With our research, we aim to determine why cells have multiple proteins capable of independently unfolding G4s, and how these proteins work together to support overall G4 maintenance. We also aim to investigate the potential for a protective effect against DNA damage inducers when repair proteins are upregulated in non-cancerous cells. Experiments were performed using *in vitro* unfolding assays to measure G4 unfolding efficiency for the proteins REV1 and FANCJ. We hypothesized that REV1 and FANCJ complement one another during G4 maintenance and would demonstrate a higher unfolding efficiency for their preferred G4 structures. Additionally, *in vivo* comet assays were used to measure DNA damage accumulation in cells overexpressing FANCJ. We expected that upregulation of the damage repair protein FANCJ would reduce damage accumulation in cells exposed to damage inducers compared to control cells exposed to

the same levels of damage inducers. These experiments will help build upon the function of REV1 and FANCJ in G4 unfolding and DNA damage resistance in healthy cells to bring a better understanding of the interaction between TLS and FA proteins in these mechanisms.

CHAPTER TWO

G-QUADRUPLEX UNFOLDING EXPERIMENTS

2.0 Introduction

G-quadruplexes present a complex genomic structure that causes replication stress by stalling replicative polymerases, which are incapable of unwinding G4 DNA. G4 structures that are not properly unfolded can lead to post-replication gaps, mutations, and overall genomic instability. Investigating the roles of repair proteins in G4 unfolding will help illuminate potential targets to suppress genomic instability and diseases such as cancer. The TLS polymerase REV1 and the FA helicase FANCJ are both capable of independently binding and unfolding G4 structures *in vitro* [5, 35]. Both proteins also exhibit a vital role in maintaining genomic stability at G4 sites *in vivo,* where the loss of either protein leads to increased mutagenesis at G4s [36, 54, 55, 56]. REV1 and FANCJ present an intriguing case because both can function independently to unfold G4s, however, they can also bind one another via the REV1-CTD and a PIP-like motif of FANCJ [2]. It is possible that the helicase and polymerase work together in G4 unfolding and replication, however, little is understood about this potential interaction. Investigating the independent and collaborative roles of these proteins in G4 unfolding will further the understanding of repair pathway proteins and may aid in the development of targeted cancer therapies.

To gain an understanding of G4 unfolding it is necessary to detect and measure G4s in a folded versus unfolded state. The vast database of G4 ligands contains useful small molecules that can serve as detection agents to identify folded and unfolded G4

DNA [49]. 3,6-bis(1-Methyl-4-vinylpyridinium) carbazole diiodide (BMVC) is a fluorescent G4 ligand, and the first capable of detecting G4s in human cells [63, 64]. BMVC was first used to detect G4 structures in telomeric sequences and was later found to interact with a parallel G4 within the cMYC promoter with a high affinity [63, 64, 65]. BMVC demonstrates an external stacking interaction with the cMYC G4, first binding the 5' end in a 1:1 ratio, and if ligand concentrations allow, secondarily binding the 3' end in a 2:1 ratio of BMVC to G4. When the ligand binds G4 DNA its fluorescence yield drastically increases compared to unbound BMVC [63, 64, 66]. In G4 detection, this specificity makes BMVC a reliable agent that has demonstrated fast and accurate discrimination in malignant cell detection based on the increase in G4 formation in cancerous cells [66]. This ligand provides a valuable research and diagnostic tool to detect and quantify both *in vitro* and *in vivo* G4 formation based on fluorescence yield.

Another G4 ligand, the heme derivative hemin (iron (III)-protoporphyrin IX), is capable of binding G4s and generating a DNAzyme with peroxidase activity. Hemin binds to folded G4s through end-stacking via pi bonds [67]. The formation of this DNAzyme offers a valuable tool in understanding G4s, as enzymatic activity can be used as a secondary measure of G4 formation within a sample.

With the available array of G4 detection methods, and known G4 unfolding proteins, it is possible to investigate the mechanisms of G4 unfolding and why multiple proteins are equipped for the job. Our research seeks to understand the role of REV1 and FANCJ in the unfolding of different conformations of G4s with and without oxidative damage. This was investigated using BMVC fluorescence assays and hemin colorimetric

assays to measure REV1 or FANCJ mediated unfolding of the G4 sequences $(TTAGGG)_4$ and $(GGGT)_4$.

2.1 Materials

2.1.1 REV1 Protein Purification

The human REV1 core (amino acids 330-833) construct pBG101-6xHis-GST-hREV1-Core was provided by Dr. Robert Eoff from the University of Arkansas. The plasmid was transformed and expressed in the BL21 (DE3) *E. coli* cell line from New England Biolabs (NEB).

The bacterial culture was started from a glycerol stock scraping placed in 125 mL LB media with 50 μg/L kanamycin and incubated overnight at 37 ˚C, shaking at 250 rpm. The culture was expanded by transferring 30 mL of growth into two 1 L LB media flasks with the same antibiotic ratio. The large-scale growth was incubated at 37 ˚C and shaken at 250 rpm until an optical density of approximately 0.5 was reached at 600 nm absorbance. Once this was reached, the cultures were induced with 1 mM IPTG per 1 L flask and incubated at 18 ˚C and 250 rpm overnight. The cultures were spun down in a centrifuge at 4,000 rpm at 4 ˚C for one hour and the pelleted cells were resuspended using lysis buffer (20 mM NaPi pH 7.5, 300 mM NaCl, 30 mM imidazole, 1 mM DTT, 5% glycerol, 1% NP40), followed by the addition of 1 mM phenylmethylsulfonyl fluoride (PMSF). The lysate was homogenized twice between 15,000-20,000 psi before being spun in a centrifuge at 18,000 rpm at 4 ˚C for one hour. The supernatant was combined with 15 mL Ni-NTA affinity chromatography beads that had been equilibrated with A1 buffer (20 mM NaPi pH 7.5, 300 mM NaCl, 30 mM imidazole, 1 mM DTT, 5% glycerol) and the bead supernatant mixture was placed on a stir plate for 1 hour at 4 ˚C. The

mixture was then run through an affinity chromatography column maintained at 4 ˚C and the flow-through was collected. The beads were washed twice with 45 mL A1 buffer, followed by two washes with 45 mL A2 buffer (20 mM NaPi pH 7.5, 30 mM NaCl, 30 mM imidazole, 1 mM DTT, 5% glycerol). The beads were then mixed with 7.5 mL B1 elution buffer (20 mM NaPi pH 7.5, 30 mM NaCl, 1 M imidazole, 1 mM DTT, 5% glycerol) for 15 minutes and the fraction was eluted. This step was repeated for a total elution volume of 15 mL. The elution was desalted using a Zebra Anion Q Spin Desalting column (Thermo Fisher Scientific) following the manufacturer provided protocol and rinsed with a 20% glycerol dialysis buffer to further purify the REV1 protein. The final elution protein concentration was determined using a NanoDrop One (Thermo Fisher Scientific) and the extinction coefficient ε280 = 77,240 $M^{-1}cm^{-1}$. Samples were processed with 4x Lammeli Dye and the purity of the protein was confirmed by running samples on a 10% acrylamide SDS-PAGE gel. Protein samples were aliquoted and flash frozen in dry ice for storage at -80 ˚C.

2.1.2 FANCJ Protein Purification

The pvL1392-GST-FANCJ-Flag construct was synthesized by VectorBuilder. Before protein expression, the construct was propagated and amplified using a baculovirus vector following the protocol from *Mechanisms of G-Quadruplex Recognition and Unfolding by the FANCJ Helicase and REV1 Polymerase* [50]. For virus propagation and amplification, $1.0x10^6$ Sf9 (Spodoptera frugiperda) cells were seeded into a single well of a six-well plate and incubated for 20 minutes at 28 ˚C. The BestBac transfection kit (Expression Systems) was used to prepare co-transfection mixtures of the baculovirus vector and the pvL1392-GST-FANCJ-Flag vector following the kit protocol.

The vectors were combined using 5 µL BestBac DNA provided by the kit and 2 µg of the FANCJ plasmid. The DNA mixture was incubated in 100 µL of kit provided transfection media for 5 minutes at 28 ˚C while 6 µL of Expres2TR transfection agent was also incubated in 100 µL of media. The DNA and transfection agent were combined and incubated for an additional 20 minutes. After this time, 800 µL of transfection media was added to the mixture. The media with the incubated Sf9 cells was removed and the transfection mixture was added to the cells for 5 hours at 28 ˚C. The media was again removed, and fresh media was added before incubation for 5 days at 28 ˚C in an atmosphere with 5% CO_2. After this time, the supernatant was isolated by centrifugation at 3,000 rpm for 5 mins and was filtered through a 0.22 µm syringe filter. The supernatant contained the Passage 0 (P0) baculovirus. To amplify the virus, 1 mL of P0 stock was added to 25 mL of suspended Sf9 cells at $2.0x10^6$ cell/mL and 95% viability. Once viability dropped to 20%, the supernatant with P1 virus was collected. An additional round of amplification was performed by adding 5 mL of P1 virus to 100 mL of Sf9 cells at $2.0x10^6$ cells/mL with 95% viability. Again, the supernatant was collected once the viability dropped to 20%. This was the amplified P2 baculovirus vector. The P2 vector was then transferred to HighFive (HF) insect cells (BTI-TN-5B1- 4) for expression by adding 10 mL of P2 virus to 200 mL of suspended HF cells at $2.0x10^6$ cells/mL and 95% viability. Once the cells reached 85% viability, they were isolated by centrifugation at 2,000 rpm for 30 mins at 4 ˚C. These cells were aliquoted into cryotubes and stored in liquid nitrogen for future use.

The GST-FANCJ-Flag protein was expressed in and purified from HF cells. Aliquoted HF cells containing the pvL1392-GST-FANCJ-Flag construct were thawed

and $2.0x10^6$ cells were seeded in 19 mL Express Five SFM media (ThermoFisher) supplemented with 18 mM L-glutamine. The culture was incubated at 28 ˚C and shaken at 90 rpm for 72 hours. The cell density was measured using an Invitrogen CountessII cell counter and when a cell density between $2.0\text{-}3.0x10^6$ cells/mL was reached, the culture was divided into four 1 L flasks each containing 250 mL of media. The cells were incubated under the same conditions for 72 hours for a larger scale growth. Once the cell density of each flask reached $2.0\text{-}3.0x10^6$ cells/mL, the media was isolated by centrifugation at 2,000 rpm for 45 minutes at 4 ˚C. The media was discarded, and the pellet was resuspended with lysis buffer (10 mM Tris-HCl pH 7.5, 130 mM NaCl, 10 mM NaPi, 5% glycerol, 1% Triton X-100). Two 50 mL Pierce Protease Inhibitor tablets and 1 mM of PMSF were added per 50 mL of lysate before mixing on a stir plate for 90 minutes at 4 ˚C. The lysate was spun down at 18,000 rpm at 4 ˚C for 30 minutes until the supernatant was no longer turbid. The supernatant was filtered through a 0.45 µm filter, then mixed with GST chromatography beads for 45 minutes. The supernatant and bead mixture was run through a column and the flow-through was collected. The beads were washed with three column volumes of GST equilibrium buffer (75 mM Tris-HCl pH 7.5, 300 mM NaCl, 5% glycerol) three times, followed by three column volumes of GST wash buffer (75 mM Tris-HCl pH 7.5, 150 mM NaCl, 5% glycerol) three times. The beads were then mixed with a half column volume of GST elution buffer (75 mM Tris-HCl pH 7.5, 150 mM NaCl, 5% glycerol, 50 mM glutathione) for 15 minutes before collection. This step was repeated for a total elution equal to the column bead volume.

The elution was then bound to FLAG antibody beads (Millipore Sigma) for 2 hours at 4 ˚C. The beads were washed with flag equilibrium buffer (25 mM Tris-HCl pH

7.5, 300 mM NaCl, 0.1% NP40, 5% glycerol) three times, followed by flag wash buffer (25 mM Tris-HCl pH 7.5, 30 mM NaCl, 0.1% NP40, 5% glycerol) three times. Lastly, the beads were mixed with flag elution buffer (25 mM Tris-HCl, 30 mM NaCl, 15% glycerol) with 100 µg/mL 3x FLAG peptide (Med Chem Express) and eluted. The purity of the eluted protein was determined by SDS-PAGE. The concentration of purified FANCJ was determined using a NanoDrop and the extinction coefficient ε280 = 181,375 $M^{-1}cm^{-1}$. Protein samples were aliquoted and flash frozen in dry ice for storage at -80 ˚C.

2.1.3 Oligonucleotides

Oligonucleotide	Sequence (5'–3')
T15-$(GGGT)_4$-Cy3	TTT TTT TTT TTT TTT/GGGT GGGT GGGT GGGT/3Cy3Sp
T15-8oxo1$(GGGT)_4$ Cy3	TTT TTT TTT TTT TTT/i8oxodG/GGT GGGT GGGT GGGT/3Cy3Sp
T15-8oxo3$(GGGT)_4$-Cy3	TTT TTT TTT TTT TTT/GG/i8oxodG/T GGGT GGGT GGGT/3Cy3Sp
T15-8oxo5$(GGGT)_4$-Cy3	TTT TTT TTT TTT TTT/GGGT G/i8oxodG/GT GGGT GGGT/3Cy3Sp
T15-$(TTAGGG)_4$-Cy3	TTT TTT TTT TTT TTT/TTA/i8oxodG/GG TTAGGG TTAGGG TTAGGG/3Cy3Sp
T15-8oxo1$(TTAGGG)_4$-Cy3	TTT TTT TTT TTT TTT/TTAGG/i8oxodG/ TTAGGG TTAGGG TTAGGG/3Cy3Sp
T15-8oxo3$(TTAGGG)_4$-Cy3	TTT TTT TTT TTT TTT/TTAGGG TTAG/i8oxodG/G TTAGGG TTAGGG/3Cy3Sp
T15-8oxo5$(TTAGGG)_4$-Cy3	TTT TTT TTT TTT TTT/TTAGGG TTAGGG TTAGGG TTAGGG/3Cy3Sp
GGGT Trap	ACCC ACCC ACCC ACCC
TTAGGG Trap	CCCTAA CCCTAA

Table 2.1: List of oligonucleotide DNA sequences: Oligonucleotide DNA used for unfolding experiments.

G4 DNA oligonucleotides were purchased and synthesized by Integrated DNA Technologies (IDT). A full list of the sequences can be found in Table 2.1. A 5' T15 ssDNA overhang was included to allow for protein binding. i8oxodG signifies oxidatively damaged guanine at the first (8oxo1), third (8oxo3), or fifth (8oxo5) guanine.

DNA concentrations were determined using a NanoDrop One (Thermo Fisher Scientific) using the molar extinction coefficients provided by IDT at 260 nm. G4 DNA samples were diluted to 10 µM stock solutions in Tris buffer containing KCl to allow proper G4 folding (10 mM Tris-HCl pH 7.5, 100 mM KCl). Samples were then heated to 95˚C for 10 minutes and slow cooled overnight to promote proper G4 folding. Samples were stored at 4 ˚C after slow cooling.

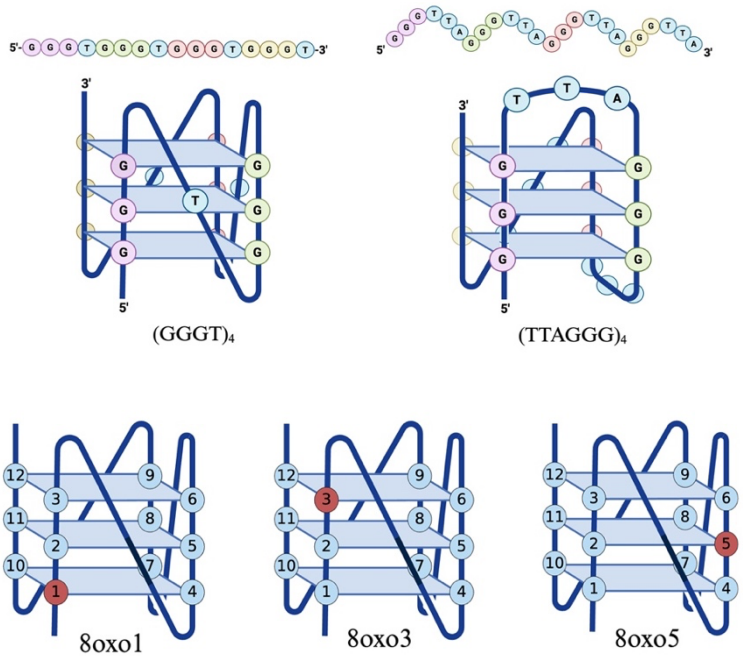

Figure 2.1: G4 constructs: The parallel $(GGGT)_4$ is depicted on the upper left and the hybrid $(TTAGGG)_4$ is depicted on the upper right. The positions of oxidative damage are shown below in the 8oxo1, 8oxo3, and 8oxo5 guanine positions within a G4 structure.

2.1.4 BMVC and Hemin Assays

For the BMVC fluorescence assay, BMVC was purchased from MedChem Express. The molecule was dissolved in DMSO and stored at a stock concentration of 10

μM at 4˚C in the dark. BMVC unfolding buffer (10 mM Tris-HCl pH 7.5, 100 mM KCl, 10 mM $MgCl_2$, 5% glycerol) was the primary reaction buffer used for all BMVC assays.

For the hemin colorimetric assay, hemin and ABTS (2,2′-azino-bis(3-ethylbenzothiazoline-6-sulfonic acid)) were purchased from MedChem Express. Hemin was dissolved in DMSO and stored at a stock concentration of 20 mM at 4 ˚C in the dark. Hemin unfolding buffer (25 mM HEPES pH 7.5, 100 mM KCl, 2 mM $MgCl_2$, 0.05% Triton-X, 1.0% DMSO) was the primary reaction buffer used for all hemin assays.

ABTS was dissolved in hemin unfolding buffer and stored at a stock concentration of 25 mM at 4 ˚C in the dark.

2.2 Methods

2.2.1 BMVC Fluorescence Assay

Assays were performed in a 96-well clear bottom plate (Greiner BioOne). BMVC unfolding buffer was used for these experiments to bring the final volume of each well to 100 μL. 250 nM of DNA and 0.1 μM of BMVC were added to each well and incubated for five minutes at 25 ˚C to allow for binding. The BMVC concentration used was determined to produce the maximum fluorescence output when bound to G4 DNA during initial titration experiments with 250 nM DNA and varying BMVC concentrations in BMVC unfolding buffer using a Cary Eclipse Fluorescence Spectrometer. After DNA incubation, varying concentrations of purified REV1 core or FANCJ were added and allowed to incubate for an additional five minutes. Next, 10 mM ATP and 250 mM trap DNA were added and incubated for an additional ten minutes. The fluorescence yield was then collected with an excitation at 458 nm and emission collection at 575 nm using a BioTek Synergy H1 Microplate Reader. The 575 nm wavelength was used based on the

previous titration trials on the Cary Eclipse Fluorescence Spectrometer and falls within the range of maximum fluorescence of BMVC at 580 nm. Three trials of eight replicates were performed for each experimental condition.

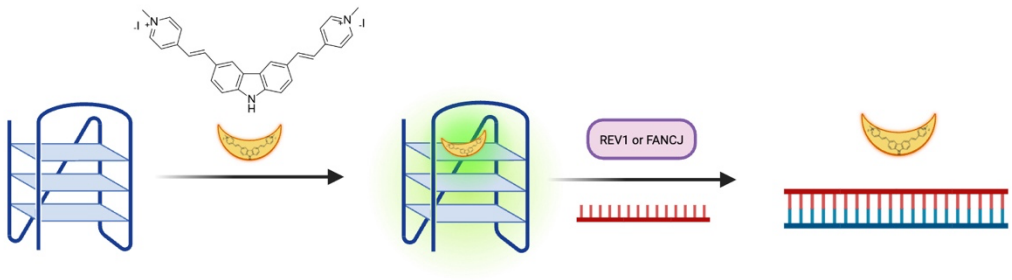

Figure 2.2: BMVC fluorescence assay: BMVC, shown in orange with its chemical structure depicted above, binds to a hybrid G4 structure via end stacking. Once bound, the BMVC fluorescence increases. As REV1 or FANCJ are added, the proteins unfold the G4 and BMVC loses its binding location. The fluorescence yield decreases as BMVC can no longer bind the G4 and refolding is prevented by the binding of the complementary trap strand shown in red.

2.2.2 Hemin Colorimetric Assay

Assays were performed in a 96-well clear bottom plate (Greiner BioOne). Hemin unfolding buffer was used for these experiments to bring the final volume of each well to 100 µL. 250 nM DNA and 250 nM hemin were added to each well containing hemin reaction buffer to allow for a 1:1 binding ratio of hemin to G4 DNA and incubated at 25 $^{\circ}$C for 30 minutes. After DNA incubation, varying concentrations of purified REV1 core or FANCJ were added and allowed to incubate for an additional five minutes. Next, 10 mM ATP and 250 mM trap DNA were added and incubated for ten minutes. Lastly, 2

mM ABTS and 2 mM H_2O_2 were added, and the plate was immediately scanned using a BioTek Synergy H1 Microplate Reader. The absorbance was collected at 420 nm based on the absorbance peak from trial scans from 400-500 nm and previous literature [68, 69]. Three trials of eight replicates were performed for each experimental condition.

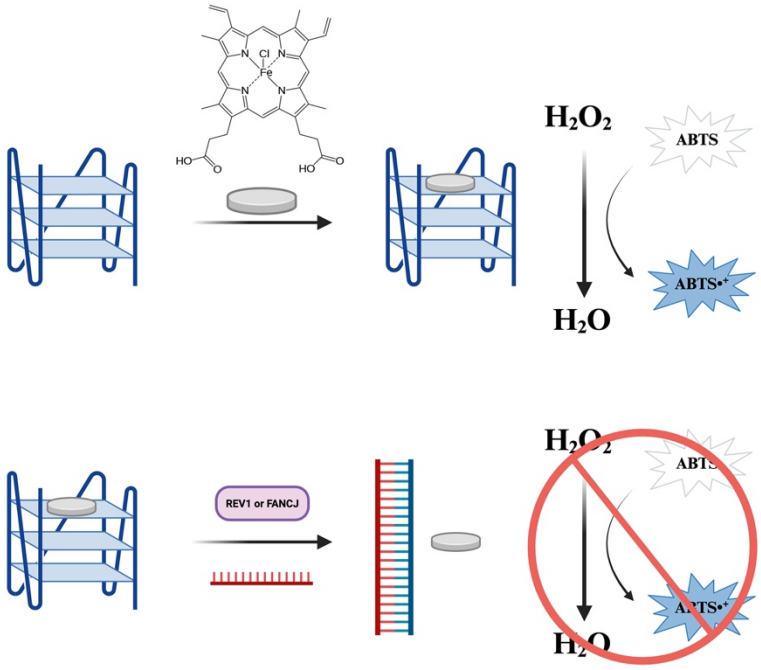

Figure 2.3: Hemin colorimetric assay: Hemin, shown in gray with its chemical structure depicted above, binds to a parallel G4 structure via end stacking. Once bound, the hemin-G4 complex functions as a DNAzyme with peroxidase activity. When properly formed, the DNAzyme catalyzes the oxidation of ABTS in the presence of hydrogen peroxide (H_2O_2). ABTS is colorless in its reduced state and blue in its oxidized state. As REV1 or FANCJ are added, the proteins unfold the G4 and peroxidase activity is lost. The oxidation of ABTS can no longer take place and no color change occurs.

2.3 Results and Conclusions

2.3.1 REV1 Unfolding G4 DNA

The unfolding of the hybrid $(TTAGGG)_4$ construct by REV1 was investigated utilizing the BMVC fluorescence assay. As varying concentrations of purified REV1 core (1-100 nM) were added to each sample, the initial BMVC signal emitted from the G4-BMVC complex decreased. This indicated successful unwinding of the G4. REV1 unfolded wild-type $(TTAGGG)_4$ with an unfolding efficiency of K_m= (8.468 ± 1.797)e-010. Unfolding of the damaged 8oxoG4s yielded greater unfolding efficiency, with the highest efficiency for $(TTAGGG)_4$ 8oxo1 with a K_m= (2.449 ± 1.218)e-011. The $(TTAGGG)_4$ 8oxo3 construct was comparable with a K_m= (5.985 ± 3.531)e-011, followed by $(TTAGGG)_4$ 8oxo5 with a K_m= (1.161 ± 0.033)e-010. This suggests that the presence of 8oxo damage increased the ability for REV1 to unfold the $(TTAGGG)_4$ sequence.

The unfolding of the parallel $(GGGT)_4$ construct by REV1 was investigated utilizing the hemin colorimetric assay. As varying concentrations of purified REV1 core (100-800 nM) were added to each sample, the amount of color present in each sample decreased with increasing concentrations of REV1. This indicated successful unwinding of the G4 and loss of DNAzyme peroxidase activity to oxidize blue ABTS into its clear oxidized state. REV1 unfolded wild-type $(GGGT)_4$ with an unfolding efficiency of K_m= (1.062 ± 0.576)e-007. Unlike the $(TTAGGG)_4$ construct, the wild-type construct had the highest unfolding efficiency, reflected by the lowest K_m value. The least efficient unfolding was of the $(GGGT)_4$ 8oxo3 construct at K_m= (4.495 ± 2.290)e-007. The $(GGGT)_4$ 8oxo5 construct had a K_m= (2.005 ± 0.252)e-007 and $(GGGT)_4$ 8oxo1, a K_m= (2.005 ± 0.252)e-007. While there is slight variation in these results, the unfolding

efficiency was not drastically different between the undamaged and damaged constructs.

Between the $(TTAGGG)_4$ and $(GGGT)_4$ constructs, REV1 exhibited higher unfolding efficiency for the hybrid $(TTAGGG)_4$. For this construct, 8oxo damage increased unfolding efficiency by REV1, while 8oxo damage within $(GGGT)_4$ demonstrated decreased unfolding efficiency compared to the undamaged G4. These results suggest that REV1 may preferentially unfold hybrid sequences, such as the telomeric sequence $(TTAGGG)_4$ and that 8oxo damage is not a significant barrier to REV1 recognition and unwinding of G4s.

REV1 was also tested in the unfolding of $(TTAGGG)_4$ and $(GGGT)_4$ with and without adenosine triphosphate (ATP) present. The hydrolysis of ATP aids in the processivity of REV1, providing the necessary energy needed to move along a strand of DNA beyond initial binding. Our assays revealed that REV1 was able to unfold the hybrid $(TTAGGG)_4$ construct in the presence of 10 mM ATP with a K_m= (8.468 ± 1.797)e-010 and without ATP with a K_m = (1.048 ± 0.751)e-09. While the presence of ATP allowed for slightly higher unfolding efficiency, REV1 was capable of unfolding the G4 without the processivity provided by ATP hydrolysis. REV1 was able to unfold the parallel $(GGGT)_4$ construct in the presence of ATP with a K_m= (1.062 ± 0.576)e-007 and without ATP with a K_m= (2.284 ± 0.212)e-007. As with $(TTAGGG)_4$, REV1 was still capable of unfolding the G4 without ATP present, but with a decrease in efficiency. The presence of ATP demonstrates a greater impact on unfolding efficiency for the more stable parallel G4. It is likely that the higher stability of this structure is not as readily unfolded by protein binding alone, while REV1 binding may be sufficient for the less

stable hybrid sequence. These findings suggest that ATP is not necessary for REV1 to interact with and resolve G4 structures but can aid in the unfolding of more stable G4s. As such, it is possible that ATP driven catalytic activity and nucleotide insertion are not the primary roles of REV1 in the unfolding and replication of G4s. Instead, REV1 may locate and destabilize these structures via binding before providing the scaffolding to recruit other TLS pols to the G4 site for the continuation of replication.

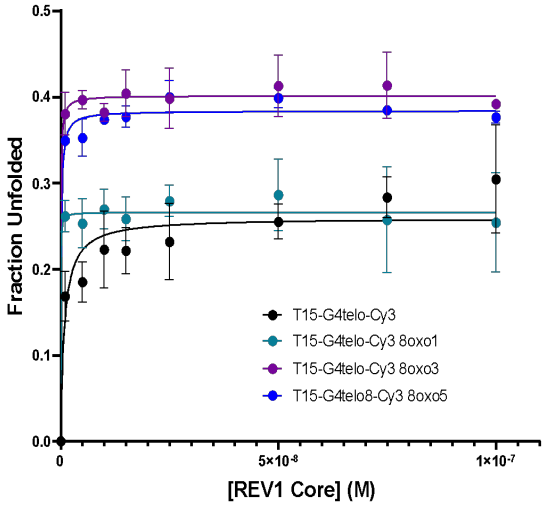

Substrate	K_m (M)	R^2
$(TTAGGG)_4$	(8.468 ± 1.797)e-010	0.9010
$(TTAGGG)_4$ 8oxo1	(2.449 ± 1.218)e-011	0.9840
$(TTAGGG)_4$ 8oxo3	(5.985 ± 3.531)e-011	0.9951
$(TTAGGG)_4$ 8oxo5	(1.161 ± 0.033)e-010	0.9905

K_m: 8oxo1 ≤ 8oxo3 < 8oxo5 < WT

Figure 2.4: $(TTAGGG)_4$ unfolded by REV1: The unfolding of the G4 sequence $(TTAGGG)_4$ and its oxidatively damaged sequences by purified REV1 core were assessed using a BMVC fluorescence assay. The fluorescence output of a sample of BMVC saturated G4 DNA was exposed to varying concentrations of REV1 (1-100 nM) and fluorescence was measured at 575 nm. The resulting values were normalized to a control sample and the relative fraction of G4s within the sample was calculated. These data were plotted in a graph as a function of varying protein concentration, seen on the left. From this data, a K_m value was generated for the undamaged and damaged sequences, seen in the table on the right. REV1 demonstrated the lowest unfolding

efficiency and highest K_m value for the undamaged $(TTAGGG)_4$ sequence. The highest unfolding efficiency was demonstrated for the 8oxo1 G4, followed by 8oxo3, then 8oxo5.

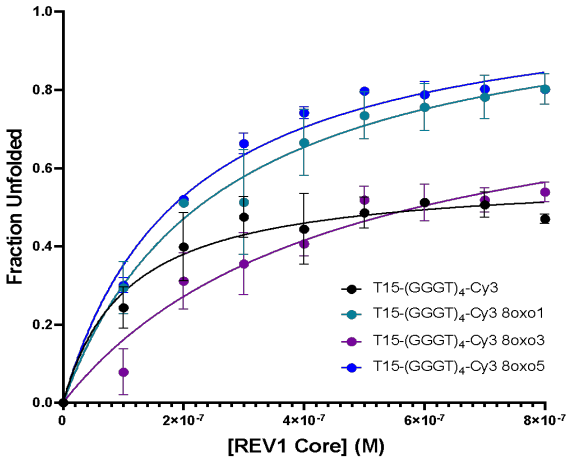

Substrate	K_m (M)	R^2
$(GGGT)_4$	(1.062 ± 0.576)e-007	0.9718
$(GGGT)_4$ 8oxo1	(2.556 ± 2.432)e-007	0.9880
$(GGGT)_4$ 8oxo3	(4.495 ± 2.290)e-007	0.9611
$(GGGT)_4$ 8oxo5	(2.005 ± 0.252)e-007	0.9857

K_m: WT ≤ 8oxo5 ≤ 8oxo1 < 8oxo3

Figure 2.5: $(GGGT)_4$ unfolded by REV1: The unfolding of the G4 sequence $(GGGT)_4$ and its oxidatively damaged sequences by purified REV1 core were assessed using a hemin colorimetric assay. A sample of hemin saturated G4 DNA in the presence of H_2O_2 and ABTS caused a color-changing oxidation reaction and produced an increase in sample absorbance with a peak at 420 nm. As a varying concentration of REV1 (100-800 nM) was added, absorbance decreased. The resulting values were normalized to a control sample without REV1 added and the relative fraction of G4s within each sample was calculated. These data were plotted in a graph as a function of varying protein concentration, seen on the left. From this data, a K_m value was generated for the undamaged and damaged sequences, seen in the table on the right. REV1 demonstrated the highest unfolding efficiency and lowest K_m value for the undamaged $(GGGT)_4$

sequence. The oxidatively damaged sequences demonstrated decreasing unfolding efficiency across 8oxo5, 8oxo1, and 8oxo3, respectively.

2.3.2 FANCJ Unfolding G4 DNA

The unfolding of the hybrid $(TTAGGG)_4$ construct by FANCJ was investigated utilizing the BMVC fluorescence assay. As with the addition of REV1, adding increasing concentrations of purified FANCJ (1-50 nM) to each sample caused the initial BMVC signal emitted from the G4-BMVC complex to decrease. FANCJ unfolded wild-type $(TTAGGG)_4$ with an unfolding efficiency of K_m= (2.546 ± 5.151)e-008. The 8oxoG4 constructs did not follow as clear of a trend as with REV1, where wild-type constructs were either most or least efficiently unfolded. In the case of FANCJ, the 8oxo3 construct had the highest unfolding efficiency of K_m = (1.135 ± 1.390)e-008. This is followed by 8oxo5 with a K_m= 1.757 ± 3.514)e-008, the undamaged sequence, and 8oxo1 which was the least efficient with a K_m= (6.108 ± 1.536)e-008. This suggests that the oxidative damage does not cause a clear shift in unfolding efficiency for the hybrid telomeric sequence unfolded by FANCJ.

The unfolding of the parallel $(GGGT)_4$ construct by FANCJ was investigated utilizing the hemin colorimetric assay. Again, as with REV1, the addition of increasing concentrations of purified FANCJ (1-40 nM) decreased the color produced by the oxidation of ABTS by the hemin-G4 DNAzyme sample. FANCJ unfolded wild-type $(GGGT)_4$ with an unfolding efficiency of K_m= (1.675 ± 0.779)e-008. The presence of oxidative damage caused a similar unfolding trend to that observed for $(TTAGGG)_4$. Like the $(TTAGGG)_4$ construct, $(GGGT)_4$ 8oxo1 had the lowest unfolding efficiency with a K_m= (1.957 ± 0.948)e-008. This was followed by the undamaged structure, then 8oxo3

with a K_m= (9.929 ± 0.715)e-009, and 8oxo5 with the highest efficiency and a K_m= (5.788 ± 2.455)e-009. As with the $(TTAGGG)_4$ construct, the 8oxo3 and 8oxo5 $(GGGT)_4$ sequences are more efficiently unfolded than the undamaged sequence, and the 8oxo1 has the least efficient unfolding by FANCJ. This may signify a stronger destabilizing effect by 8oxo3 and 8oxo5, allowing FANCJ to unwind the G4 DNA easier, while 8oxo1 on the 5' guanine may complicate G4 unfolding by blocking processivity of the 5'-3' helicase.

Between the $(TTAGGG)_4$ and $(GGGT)_4$ constructs, FANCJ exhibited higher unfolding efficiency for the parallel $(GGGT)_4$, although with less distinct of a preference from that seen with REV1. Oxidative damage did not exhibit the same effects on FANCJ unfolding the parallel and hybrid G4s as that seen by REV1. 8oxo3 and 8oxo5 damage seemed to increase unfolding efficiency for both sequences, as seen with REV1 unfolding $(TTAGGG)_4$. 8oxo1, however, seemed to decrease unfolding efficiency by FANCJ. Overall, these results suggest that FANCJ may have a slight preference for parallel G4s such as $(GGGT)_4$, and that oxidative damage does not prevent unfolding but may alter efficiency depending on its location within a G4.

FANCJ was also tested in the unfolding of $(GGGT)_4$ with and without ATP. The hydrolysis of ATP allows FANCJ to slide along a DNA sequence to separate dsDNA. We found that FANCJ was able to unfold the parallel $(GGGT)_4$ construct in the presence of 10 mM ATP with a K_m= (1.675 ± 0.779)e-008 and without ATP with a K_m= (3.055 ± 0.688)e-009. Unlike with REV1, the presence of ATP hindered unfolding efficiency for FANCJ with $(GGGT)_4$. It is possible that the presence of ATP increased molecular motor activity to a degree that hindered FANCJ from steadily binding to the short G4 oligonucleotides to unfold them.

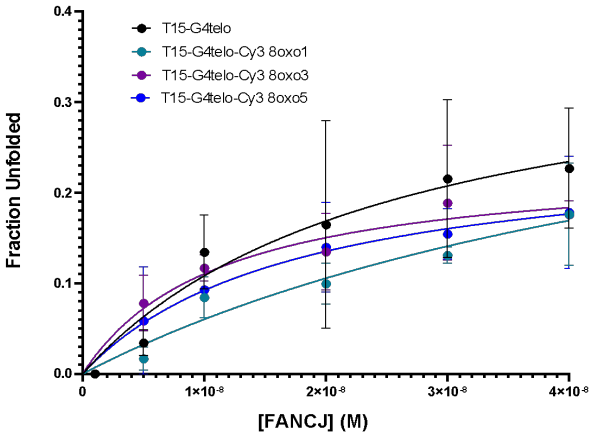

Substrate	K_m (M)	R^2
$(TTAGGG)_4$	(2.546 ± 5.151)e-008	0.9577
$(TTAGGG)_4$ 8oxo1	(6.108 ± 1.536)e-008	0.9529
$(TTAGGG)_4$ 8oxo3	(1.135 ± 1.390)e-008	0.9561
$(TTAGGG)_4$ 8oxo5	(1.757 ± 3.514)e-008	0.9888

K_m: 8oxo3 ≤ 8oxo5 ≤ WT ≤ 8oxo1

Figure 2.6: $(TTAGGG)_4$ unfolded by FANCJ: The unfolding of the G4 sequence $(TTAGGG)_4$ and its oxidatively damaged sequences by purified FANCJ were assessed using a BMVC fluorescence assay. Varying concentrations of FANCJ (1-50 nM) were added to $(TTAGGG)_4$ DNA saturated with BMVC and fluorescence was measured at 575 nm. The resulting values were normalized to a control sample and the relative fraction of G4s within the sample was calculated. These data were plotted in a graph as a function of varying protein concentration, seen on the left. From this data, a K_m value was generated for the undamaged and damaged sequences, seen in the table on the right. FANCJ demonstrated the lowest unfolding efficiency for the 8oxo3 G4, followed by 8oxo5, undamaged, and 8oxo1.

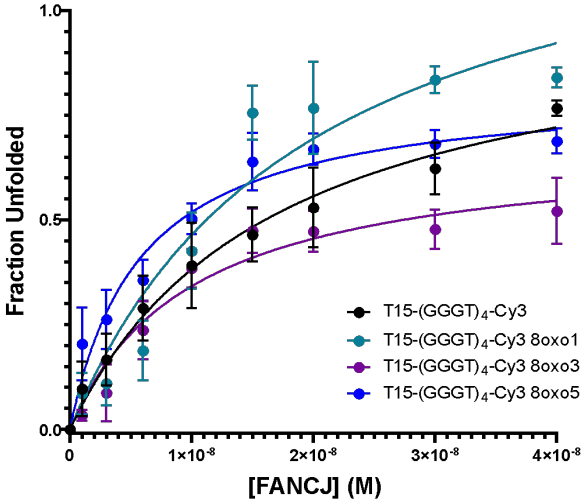

Substrate	K_m (M)	R^2
$(GGGT)_4$	(1.675 ± 0.779)e-008	0.9876
$(GGGT)_4$ 8oxo1	(1.957 ± 0.948)e-008	0.9381
$(GGGT)_4$ 8oxo3	(9.929 ± 0.715)e-009	0.9600
$(GGGT)_4$ 8oxo5	(5.788 ± 2.455)e-009	0.9695

K_m: 8oxo5 < 8oxo3 < WT ≤ 8oxo1

Figure 2.7: $(GGGT)_4$ unfolded by FANCJ: The unfolding of the G4 sequence $(GGGT)_4$ and its oxidatively damaged sequences by purified FANCJ were assessed using a hemin colorimetric assay. As increasing concentrations of FANCJ (1-40 nM) were added to a hemin-G4 DNAzyme sample with H_2O_2 and ABTS, G4s were unfolded, and peroxidase activity was impaired. This resulted in a decrease in color change as ABTS was not as readily oxidized. The color change was measured with an absorbance peak at 420 nm. The resulting absorbance values were normalized to a control sample without FANCJ added and the relative fraction of G4s within each sample was calculated. These data were plotted in a graph as a function of varying protein concentration, seen on the left. From this data, a K_m value was generated for the undamaged and damaged sequences, seen in the table on the right. FANCJ demonstrated the lowest unfolding efficiency for the 8oxo5 G4, followed by 8oxo3, undamaged, and 8oxo1.

2.3.3 Conclusions

Overall, REV1 and FANCJ both demonstrated effective unfolding for the hybrid $(TTAGGG)_4$ and parallel $(GGGT)_4$ G4 constructs, as well these sequences with oxidative

damage in the first, third, or fifth guanine position. REV1 unfolded the hybrid sequence and the 8oxoG4 constructs with an overall higher efficiency than the unfolding of the parallel sequences. REV1 also unfolded the hybrid sequences with a higher efficiency than FANCJ with these sequences. While FANCJ exhibited similar unfolding efficiencies for both hybrid and parallel structures, the helicase had a higher efficiency for the $(GGGT)_4$ construct compared to REV1. These findings suggest that REV1 and FANCJ may have a complementary role in G4 maintenance where REV1 targets hybrid G4s, while FANCJ targets parallel sequences. It is also interesting to note that neither protein required ATP for G4 unwinding, suggesting that binding alone may be sufficient for initial unfolding.

2.4 Discussion and Future Directions

The unfolding of G4s is vital for DNA replication to proceed unhindered in a dividing cell. REV1 and FANCJ are two repair proteins specialized to recognize, bind, and unfold G4s and are necessary in processivity past these structures [36, 54, 55, 56]. Despite knowing that these proteins are necessary, their interaction with different G4 structures, and with each other, is not yet well understood. To expand this knowledge, we investigated REV1 or FANCJ mediated unfolding of the hybrid telomeric sequence $(TTAGGG)_4$ and the parallel sequence $(GGGT)_4$ through BMVC fluorescence assays and hemin colorimetric assays. In addition to this, the presence of oxidative damage on the first, third, or fifth guanine was generated to investigate the impact of 8oxo damage on protein mediated G4 unfolding.

Our study revealed that REV1 demonstrates a preference for the hybrid $(TTAGGG)_4$ compared to the parallel $(GGGT)_4$ G4 through more efficient unfolding of

the hybrid structure based on lower K_m values. Additionally, REV1 is capable of unfolding oxidatively damaged G4s of both sequences. 8oxo $(TTAGGG)_4$ constructs yielded higher K_m values compared to the undamaged sequence, indicating a more efficient unwinding, potentially due to the lower stability of the sequence. 8oxo $(GGGT)_4$ resulted in the opposite, where the undamaged sequence was more efficiently unfolded by REV1. Unfolding assays with and without ATP revealed that REV1 is capable of unfolding G4s with and without catalytic activity, likely as the result of recognition and binding which relaxes the G4 structure. Taken together these results suggest that REV1 is capable of unfolding G4s with and without damage primarily due to the initial binding of the polymerase to the G4 structure. While the presence of ATP may aid in this unfolding, it is not essential.

The investigation of FANCJ with the $(TTAGGG)_4$ and $(GGGT)_4$ constructs showed that FANCJ was capable of unfolding both structures with and without 8oxo damage. While unfolding efficiencies were comparable between G4 constructs, FANCJ exhibited a higher unfolding efficiency for the $(GGGT)_4$ structure compared to REV1. This suggests that the two proteins play a complementary role in G4 unfolding by preferentially targeting the sequences they are most efficient at unfolding. FANCJ was investigated with $(GGGT)_4$ with and without ATP and found to be able to unfold the construct without ATP present with a higher efficiency than with ATP. It is possible that ATP hydrolysis activates FANCJ such that the protein is not capable of as stable a binding to the G4.

Overall, our unfolding study helps direct the investigation of the individual specificity and unfolding capacity of REV1 and FANCJ for parallel and hybrid G4

sequences with and without oxidative damage. To further this study, expanding the G4 constructs to include anti-parallel structures as well as other known parallel and hybrid sequences such as the anti-parallel TBA (thrombin binding aptamer) sequence or the parallel c-MYC sequence would be beneficial to compare results across multiple sequences and conformations. While expanding the sequences used would provide a broader knowledge base about REV1 and FANCJ interactions with G4s, there is a limitation with the use of BMVC and hemin assays. These unfolding assays provide secondary measurements used to infer and calculate unfolding. While this can be useful for a general sense of unfolding capacity, the assays do not reveal kinetic mechanisms of protein interactions with G4s. In order to expand upon our findings, a biophysical approach utilizing C-Trap optical tweezer microscopy would allow the direct detection of G4 unfolding [70]. Previous studies have demonstrated G4 binding between optical traps to study their unfolding or replication [70, 71, 72]. In such an experiment, G4 DNA is tethered between two polystyrene beads with different coatings which allow for DNA handle binding. These beads are caught in trapping lasers which can be moved to manipulate the tethered DNA, detecting distance while a force detector measures the tension on the strand. This process is performed under a confocal microscope which allows a clear visual of the beads, and if a fluorescent tag is in use, of the DNA as well.

G4s vary in their stability, which affects the force required to unfold them. Experimental studies have demonstrated a range of forces required to unfold different G4s within RNA or DNA from 23 pN for the telomeric RNA G4 TERRA to 54 pN for the parallel Myc2345 DNA G4 [70, 71, 72]. Additionally, G4 stabilization increases the force needed to unfold a G4 [70, 71]. The success of experiments utilizing optical

tweezers to manipulate and measure G4 DNA prompted our lab to seek this instrument out as a direct way to investigate REV1 and FANCJ mediated G4 unfolding. Thus far in this endeavor we have annealed the $(TTAGGG)_4$ sequence between two DNA handles (~2.5 kilobases each, ~5 kilobases total) from the Lumicks Hairpin labeling and tethering kit. These handles bind to anti-digoxigenin and streptavidin coated polystyrene beads via a 5'-digoxigenin tag and 3'-biotin tag. We have successfully formed tethers that enable the force detection as our G4 DNA is mechanically stretched, however, have not yet optimized the construct for detection of the unfolding event. In the future, we aim to measure G4 unfolding using fluorescently tagged REV1 and FANCJ to provide valuable insight in the selectivity, efficiency, and mechanisms of unfolding by these proteins.

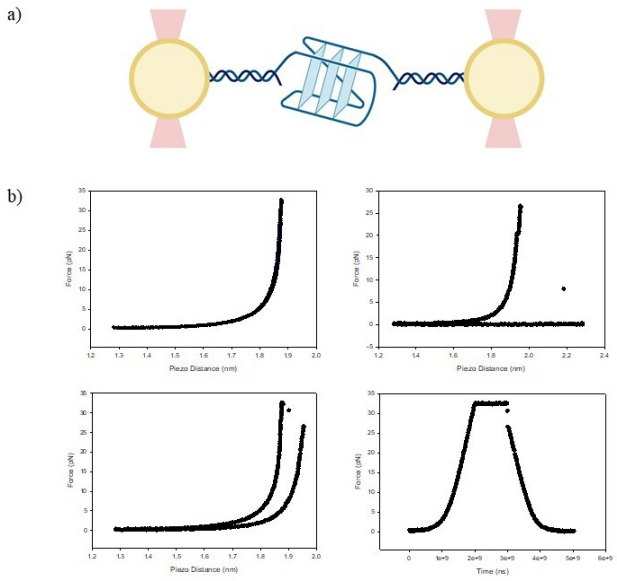

Figure 2.8: Example force-distance curves from $(TTAGGG)_4$: a) Schematic of a hybrid G4 tethered between two beads (yellow) which are trapped in optical tweezer lasers (pink). The beads can be manipulated by moving the lasers apart or together to add

tension or relax the DNA strand. In this way, the tethered G4 can be mechanically unfolded. b) C-Trap optical tweezers were used to generate force distance curves from several G4 DNA tethers through pulling and relaxation of the tether. The top left graph depicts the force distance curve from a pull to ~33 pN without G4 unfolding. The top right shows a G4 tether breaking at ~27 pN and the force falling to zero. The bottom graphs show the force-distance curve and force-time plot of a potential G4 relaxing at ~33 pN, demonstrated by the quick transition to a lower force ~27 pN. As the distance is decreased again, the structure reverses, potentially signifying G4 refolding upon return to a lower force.

While REV1 and FANCJ can interact *in vitro,* it has not yet been confirmed that these proteins co-localize at G4 sites. As such, an additional direction our lab seeks to pursue is the investigation of REV1 and FANCJ interactions *in vivo* by visualizing labeled proteins within a cell. Utilizing confocal microscopy it will be possible to visualize the localization of these proteins relative to BMVC stained G4s if they are labeled with distinctly colored fluorescent tags. In our lab we have generated a protocol for FANCJ-mNG transfection yielding around 20% efficiency. We have achieved similar efficiency with the transfection of the REV1-CTD but have not yet transfected the full length REV1 with a high enough yield for localization experiments. As we proceed with these experiments, we will be able to determine if REV1 and FANCJ participate in collaborative G4 unfolding based on their localization to the same G4 sites or different sites.

Continuing the investigation of REV1 and FANCJ continues to intrigue our lab due to its relevance in the understanding of DNA damage repair pathway interactions,

action outside of typical pathways, and G4 unfolding and replication to promote genomic stability and suppress cancer formation.

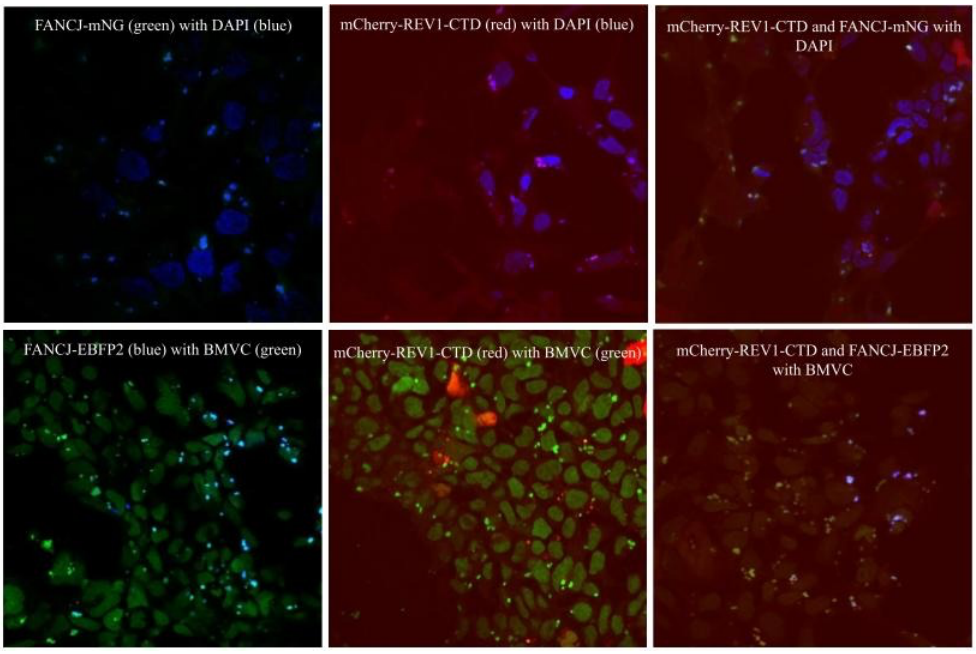

Figure 2.9: Preliminary localization of FANCJ and the REV1-CTD: HEK293 cells were transfected with FANCJ-mNG (green), FANCJ-EBFP2 (blue), or mCherry-REV1-CTD (red) and stained with the nucleus stain DAPI (blue) or the G4 stain BMVC (green). Bright puncta on each image depict overlays of transfected protein and DNA stain, revealing localization to the nucleus or a G4 structure. These spots can be seen for each construct, however, FANCJ localizes to nuclear DNA and G4s, while mCherry-REV1-CTD is more diffused across the entire cell.

CHAPTER THREE

DNA DAMAGE EXPERIMENTS

3.0 Introduction

DNA damage can lead to genomic instability, a hallmark of cancer. DNA repair pathways are able to suppress mutagenesis and improve cell survival. Intriguingly, both the upregulation and downregulation of repair proteins can promote cancer cell viability [15, 16, 51, 56]. The downregulation or impairment of these pathways allows damage to go unrepaired and results in mutagenesis and increased risk of cancer formation [51, 56]. Conversely, in cancerous cells, DNA damage repair proteins are often upregulated and aid in cancer survival by repairing enough damage caused by chemotherapies or mutagenic changes to suppress senescence signaling [15, 16]. With these properties, the delicate balance of DNA repair becomes an important element to highlight within cancer research.

One experimental approach to study DNA damage utilizes the comet assay. To run a comet assay, cells are adhered to a slide in an agarose solution and lysed open before exposing their genomic contents to an unwinding buffer. Once the DNA is unwound, the slides are placed in an electrophoresis chamber to separate DNA fragments based on size. After staining and imaging, cell nuclei with minimal DNA damage appear rounded. Cells with increasing damage gain a “comet tail” where fragments of DNA migrate away from the cell nucleus due to their smaller size. This method of analysis allows the detection and quantification of damage from double-stranded and single-stranded DNA breaks in cells. To study the impact of DNA repair proteins on DNA

damage, the protein of interest can be upregulated or downregulated in cells exposed to damage inducers. The fragility of the balance between over and under expression of DNA repair proteins is an important topic to investigate as scientists seek to understand the interplay between damage repair pathways and cancer formation.

Our research aims to determine the effect of repair protein overexpression in non-cancerous cells exposed to damage inducers. In this dissertation, the FA repair protein FANCJ was assessed in HEK293T cells exposed to varying concentrations of either menadione or bleomycin.

3.1 Materials

3.1.1 Cell Culture

Human embryonic kidney (HEK) 293T cells were purchased from ATCC. All experiments were performed from passage 9 cells stored in liquid nitrogen until the time of use. All materials used were tissue culture grade sterilized. HyClone DME/F-12 1:1 media with 2.50 mM L-glutamine and 0.1 mM HEPES was purchased from Cytiva and supplemented with 10% fetal bovine serum (FBS) and 60 µg/mL penicillin and streptomycin antibiotics. HyClone phosphate buffered saline (PBS) with 0.0067 M PO_4 without calcium or magnesium was also purchased from Cytiva.

3.1.2 Transfection

Fluorescently tagged FANCJ-EBFP2 and FANCJ-mNG pcDNA3.1 constructs were synthesized by VectorBuilder. These plasmids were transformed into and purified from Neb5α and Neb10*β E. coli* cells (New England Biolabs) which were stored at -80 $^{\circ}$C until the time of use. The pcDNA3.1 plasmids were purified using the NucleoBond

Xtra Midi plasmid DNA purification kit (Macherey-Nagel), following the June 2022/ Rev.17 manufacturer protocol.

Tissue culture grade polyethylenimine (PEI) and Opti-MEM reduced serum medium (Gibco) with HEPES, 2.4 g/L sodium bicarbonate, and L-glutamine were used for transfection of the DNA plasmids into HEK293T cells for protein expression.

3.1.3 Alkaline Comet Assays

The damage inducer menadione was dissolved in DMSO at a concentration of 2 mM and stored at -20 ˚C. Bleomycin hydrochloride (MedChemExpress) was dissolved in PBS at a concentration of 1mg/mL and stored at -20 ˚C.

To lyse cells, CometAssay Lysis Solution (R&D systems) was purchased. All other buffers were made using ultra-pure type I water (MQ) (ThermoScientific Barnstead Smart2Pure) and were sterilized using a 0.22 µm filter.

Slide preparation entailed coating slides with a 1% low melt agarose solution dissolved in MQ water. The agarose solution was heated until boiling, then slides were dipped into the agarose and excess solution was wiped off the back of the slides. The slides were dried flat overnight before being stored at 25 ˚C.

To stain cellular DNA, SYBR Gold (Thermo Fisher Scientific) and DAPI (Thermo Fisher Scientific; D1306) were used. Both stains were stored at -20 ˚C in the dark until use. 10,000x SYBR gold in DMSO was diluted in TE buffer (10 mM Tris-HCl pH 7.5, 1 mM EDTA) in a 1:30,000 dilution for staining. DAPI was diluted in filtered MQ water to a concentration of 1 µg/mL for staining.

3.2 Methods

3.2.1 Cell Culture and Transfection

Passage 9 HEK293T cells stored in liquid nitrogen were thawed and seeded at $3.0x10^5$ cells/mL into a 60 mm petri dish in 3 mL DME/F-12 media with 10% FBS and penicillin/streptomycin antibiotics. The cells were cultured for 48 hours at 37 ˚C in an atmosphere of 5% CO_2 until confluency was reached around $2.0x10^6$ cells/mL. Cells were then rinsed with PBS and released from the dish using 0.25% trypsin and a cell scraper before being split to a 6-well plate at $3.0x10^5$ cells/mL with 2 mL total per well. Cells were cultured for 24 hours in antibiotic free DME/F-12 media with 10% FBS prior to transfection and 48 hours prior to a comet assay.

To transfect the HEK293T cells, 4 µg purified pcDNA3.1 DNA and 4 µg PEI were separately combined with 50 µL Opti-MEM media and incubated for five minutes at 25 ˚C. The DNA and PEI media mixture were then combined and incubated together for 20 minutes at 25 ˚C to allow the PEI to coat the DNA. After this time, the mixture was added to one well of the 6-well plate containing cells incubated for 24 hours and was incubated for an additional 24 hours. After 48 hours total incubation in the 6-well plate, cells reached a density of $2.0x10^6$ cells/mL and the transfection efficiency could be assessed using an Agilent BioTek Cytation1 imager using the appropriate imaging LED cube. Transfection efficiency of FANCJ-mNG was optimized at 4% of cells expressing the transfected protein. FANCJ-EBFP2 was optimized at 20% of cells expressing the transfected protein. After 48 hours of incubation in the 6-well plate, control cells or cells transfected at 24 hours were ready for use in the comet assay.

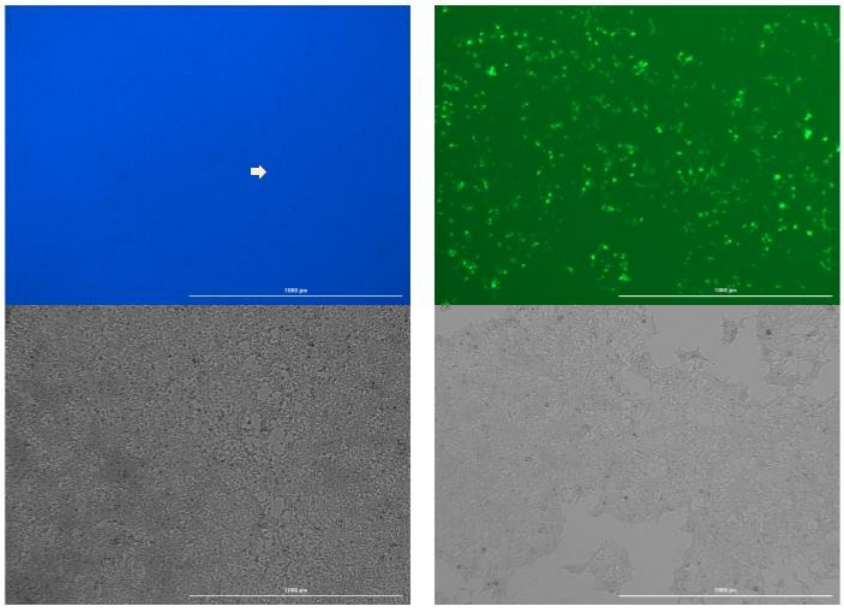

Figure 3.1: Transfection of FANCJ-EBFP2 and FANCJ-mNG: Depicted on the left are HEK293T cells 24 hours post transfection with FANCJ-EBFP2. The arrow points to the faint blue puncta of a transfected cell imaged using a DAPI filter (ex. 377 nm, em. 447 nm). Transfection efficiency was optimized with only 4% of the total cell count expressing FANCJ-EBFP2. Depicted on the right are HEK293T cells transfected with FANCJ-mNG and imaged using a GFP filter (ex. 469 nm, em. 525 nm). The transfection efficiency was optimized at 20% of the total cell count expressing FANCJ-mNG. Images were captured with the Agilent BioTek Cytation1 imager through the Gen5 Microplate reader and Imager Software 3.10.

3.2.2 Alkaline Comet Assays

Alkaline comet assays were used to assess DNA damage in cells exposed to either menadione or bleomycin. Menadione is a synthetic vitamin K derivative (K3) that generates reactive oxygen species (ROS) which induce both ssDNA and dsDNA breaks

in an increasing proportion to menadione concentration and ROS production [73, 74, 75]. Bleomycin is a natural antibiotic and approved chemotherapeutic drug capable of causing ssDNA and dsDNA breaks, with dsDNA breaks being the primary cause for cytotoxicity [76, 77]. HEK293T cells were treated with media containing menadione or bleomycin at concentrations ranging from 0.001-10 μM for two hours to induce DNA damage [74, 78]. These concentrations are considered low for each damage inducer but have been determined to cause detectable damage without causing significant cell death [74, 77, 78]. After treatment, cells were processed for alkaline comet assays, which detect single and double-stranded breaks [79, 80].

To prepare cells for the assay, the treatment media was removed, and the cells were rinsed with PBS. The cells were removed from 6-well culture plates using 0.5 mL 0.05% trypsin per well, which was incubated with the cells for 3 minutes then diluted with 1.5 mL DME/F-12 media. Remaining adherent cells were removed with a cell scraper and suspended in the media. Each cell suspension was transferred to a 5 mL tube and spun at 3,000 rpm for 5 minutes in a centrifuge. The media was removed, and cells were rinsed with 2 mL PBS then spun again. This step was repeated for a total of two rinses. The cell count was taken using an Invitrogen CountessII machine using Trypan blue stain and the cells were diluted in PBS to a concentration of $1.0x10^6$ cells/mL. Diluted cells were mixed in a 1:100 ratio with 1% agarose dissolved in PBS. 75 μL of the agarose cell suspension was transferred to each well of a 1% low melt agarose coated slide following a two well CometSlide template (R&D systems). A coverslip was placed over each well and the slides were chilled flat at 4 ˚C for 10 minutes. The coverslips were removed after the agarose solidified.

Slides were placed in chilled lysis buffer for 60 minutes at 4 ˚C then transferred to an alkaline unwinding solution (200 mM NaOH, 1mM EDTA) for 20 minutes at 25 ˚C. Slides were then placed in a Trevigen CometAssay ESII electrophoresis chamber, covered with 850 mL of chilled alkaline electrophoresis buffer (200 mM NaOH, 1 mM EDTA), and a voltage of 21 V was applied for 30 minutes on ice. After this time, slides were rinsed in filtered MQ water for five minutes twice, followed by a single rinse in 70% ethanol for five minutes. Slides were then dried at 37 ˚C for 15 minutes or until the ethanol was fully dried and the agarose cell mixture was fixed to the slides. Slides were stored in the dark in a desiccator jar until DNA staining and imaging the next day.

Control cells and cells transfected with FANCJ-EBFP2 were stained with SYBR gold. 500 µL of the solution was placed on each well and incubated for 30 minutes in the dark. Excess stain was removed, and slides were rinsed in MQ water for 2 minutes then dried at 37 ˚C before imaging. Control cells and cells transfected with FANCJ-mNG were stained with DAPI. 20 µL of DAPI solution was placed on each well and covered with a cover slip. Slides were incubated at 25 ˚C for 5 minutes in the dark before imaging.

3.2.3 Imaging and Analysis

Comets were imaged using an Agilent BioTek Cytation1 and Gen5 Microplate Reader and Imager Software (BioTek version 3.10). Slides stained with SYBR gold (ex. 300 and 469 nm, em. 537 nm) and were imaged using a GFP filter (ex. 469 nm, em. 525 nm) [81]. Slides stained with DAPI (ex. 341 nm, em. 452 nm) and were imaged using a DAPI filter (ex. 377 nm, em. 447 nm) [82]. Images were captured then processed using the Trevigen Comet Analysis Software which identifies comets, calculates the statistics for each cell such as the percentage of DNA in the tail, and generates averaged data for

all of the cells scanned in a well. These results quantify DNA damage for effective comparison.

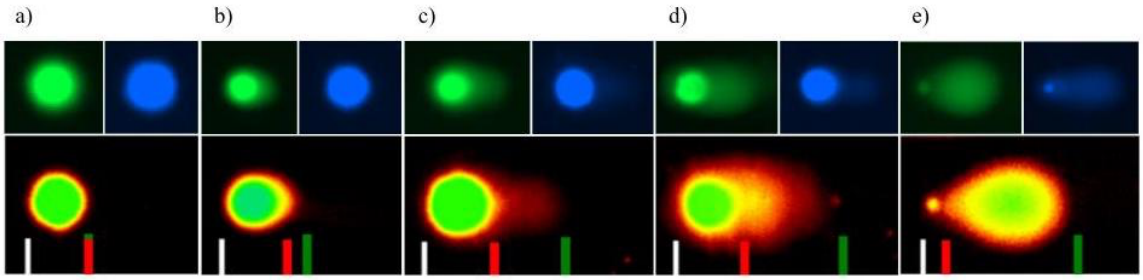

Figure 3.2: Example comets: Comet images seen in green and blue above are the raw images taken using GFP and DAPI filters respectively. Below the raw images are Trevigen Comet Analysis Software overlays for a comet corresponding to that level of damage. The white and red bars mark the start and end of the comet head. The comet tail is between the red and green bars. The software calculates the percentage of DNA in the tail, which is the quantification of DNA damage. A higher percentage of DNA in the tail signifies more damage. Pictured above are example comets with a) 1% DNA in the tail b) 10% DNA in the tail c) 20% DNA in tail d) 40% DNA in tail e) 97% DNA in tail. Image a) is an undamaged cell, while image e) is a "hedgehog" comet with almost all DNA in the tail and often signifies an apoptotic cell [83].

3.3 Results and Conclusions

3.3.1 Menadione Treatment

Control HEK293T cells treated with 0.001-10 µM of the DNA damage inducer menadione exhibited a high level of baseline damage utilizing SYBR Gold stain. SYBR Gold is known to be a very sensitive DNA ligand, which likely contributed to the

elevated damage recorded [81]. Results were gathered from 3-4 independent trials with 500+ comets detected per trial. Unexpectedly, increasing levels of menadione did not yield a clear trend in increasing DNA damage. Instead, the highest concentrations of menadione at 1 and 10 μM exhibit the lowest percentage of DNA in the comet tail at 25.03 and 25.07%. The largest amount of damage was recorded for 0.01 μM menadione at 29.42%. Cells transfected with the FANCJ-EBFP2 construct exhibited an optimized transfection efficiency at 4% cells expressing the protein. When these cells were treated with 0.001-1 μM menadione, the overall damage recorded was reduced compared to control cells. Opposite of the control cells, FANCJ-EBFP2 cells exhibited the lowest level of damage for 0.01 μM menadione with 16.15% DNA in the tail. The highest level of damage was seen in transfected cells exposed to 0.1 μM menadione with 20.85% DNA in the tail. Untreated cells had the second to lowest damage with 16.48% DNA in the tail. It is likely that menadione treatment within a 0.001-10 μM range was not sufficient to generate measurable changes in DNA damage within HEK293T cells. Additionally, treatment conditions below the threshold for significant damage induction may have triggered DNA repair mechanisms, such that damage was suppressed even beyond that of the baseline level of damage in untreated cells. The transfection of FANCJ-EBFP2 seemed to have a protective effect from DNA damage compared to untransfected cells. It is unlikely that FANCJ upregulation is responsible for this response because of the low transfection efficiency of only 4%. Instead, it is possible that transfection reagents also triggered DNA repair pathways which suppressed damage accumulation upon exposure to menadione.

Cells stained using the less sensitive DAPI DNA stain showed an overall lower baseline level of damage for both untransfected and transfected cells compared to those imaged using SYBR Gold, indicating the less sensitive nature of the stain. Control cells imaged with DAPI exhibited a similar decline in damage for cells treated with higher concentrations of menadione with 10.56 and 10.06% DNA in the comet tails for 1 and 10 μM respectively. Strangely, the untreated cells demonstrated the highest level of damage with an average of 12.54% DNA in the comet tail. Cells were transfected with FANCJ-mNG with a transfection efficiency of 20%. When transfected cells were exposed to 0.001-10 μM menadione, a trend was observed with damage decreasing from 0 to 1 μM treatments. The lowest damage was seen at 9.74% for 1 μM menadione. The highest damage was recorded for the 10 μM treatment at 11.22%. Like the HEK293T cells imaged with SYBR Gold, it is likely that the concentration range of menadione tested was low enough to trigger DNA repair pathways while not producing high levels of DNA damage. This would explain the decrease in damage seen compared to the untreated controls. Additionally, the transfection with 20% efficiency also seemed to have a slight protective effect for DAPI stained cells compared to untransfected cells. The slight decrease in DNA damage for cells treated with 0.001-1 μM menadione may be the effect of transfection reagents activating damage response pathways or from the higher transfection efficiency and overexpression of FANCJ. The increase of damage seen for transfected cells exposed to 10 μM menadione indicates that transfection increased cell susceptibility to damage at higher treatment concentrations.

Taken together, these results demonstrate the high sensitivity of SYBR Gold for DNA damage based on the overall elevation in damage recorded compared to DAPI

stained cells under the same treatment conditions. While menadione treatments from 0.001-10 µM did not exhibit extensive damage accumulation, the slight decline in DNA damage observed with menadione treatment was unexpected. This decrease in damage may indicate the activation of damage suppression systems within cells exposed to menadione at concentrations which are insufficient to cause extensive damage or cell death. Additionally, transfection seemed to have a slight protective effect for HEK293T cells for both low and higher transfection efficiency of FANCJ plasmids at 4% and 20%. The decline in damage for both low and higher-efficiency transfections suggests that the transfection reagents may have a protective effect themselves, or trigger damage response pathways which protect cells when they are exposed to menadione.

Menadione (µM)	% DNA in Tail Control (SYBR Gold)	% DNA in Tail FANCJ-EBFP2 (SYBR Gold)	% DNA in Tail Control (DAPI)	% DNA in Tail FANCJ-mNG (DAPI)
0 (No FANCJ)	27.19 ± 5.05	16.48 ± 2.73	12.54 ± 3.51	10.15 ± 1.72
0	-	18.58 ± 3.83	-	11.08 ± 0.45
0.001	26.04 ± 6.94	17.84 ± 4.42	11.40 ± 2.62	10.16 ± 0.41
0.01	29.42 ± 8.05	16.15 ± 4.48	10.97 ± 2.04	10.05 ± 0.95
0.1	27.28 ± 9.40	20.85 ± 0.87	11.54 ± 2.70	9.79 ± 1.01
1	25.03 ± 8.18	17.45 ± 1.42	10.56 ± 2.18	9.74 ± 0.98
10	25.07 ± 6.70	-	10.06 ± 1.49	11.22 ± 1.98

Table 3.1: Damage results for HEK293T cells with menadione: The percent DNA in the comet tail is used to determine the extent of DNA damage of cells transfected with either FANCJ-EBFP2 (4% transfection efficiency) or FANCJ-mNG (20% transfection efficiency) compared to untransfected controls.

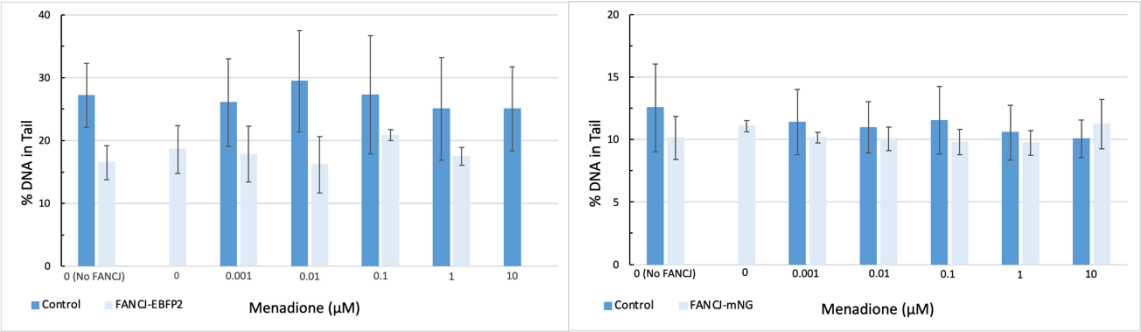

Figure 3.3: HEK293T cells with menadione treatment: The graph on the left depicts the untransfected control cells compared to FANCJ-EBFP2 transfected cells exposed to 0, 0.001, 0.01, 0.1, 1, and 10 μM menadione. These cells were imaged using SYBR Gold stain. The graph on the right depicts untransfected control cells compared to FANCJ-mNG transfected cells exposed to the same concentrations of menadione. These cells were imaged using DAPI stain. For both conditions, a decrease in damage is seen for transfected cells compared to their respective control for all but the FANCJ-mNG cells treated with 10 μM menadione. It is possible that the decreased damage seen for treated cells is due to the activation of endogenous damage suppression systems.

3.3.2 Bleomycin Treatment

Like the cells treated with menadione, control HEK293T cells treated with 0.001-10 μM of bleomycin exhibited a high level of baseline damage utilizing SYBR Gold stain. This is again likely due to the high sensitivity of the stain. Results were gathered from 3-4 independent trials with 500+ comets detected per trial. Unlike menadione treatment, increasing concentrations of bleomycin exhibited an increasing level of DNA damage by increased DNA in the comet tail. Control cells stained with SYBR Gold yielded increasing DNA damage from 0-10 μM with a low of 34.94% DNA in the tail for

0 μM bleomycin and a high of 64.26% DNA in the tail for 10 μM bleomycin. There was an exception at 0.1 μM bleomycin which exhibited the overall lowest damage with 34.56% DNA in the tail. The FANCJ-EBFP2 transfected cells treated with 0-1 μM bleomycin also demonstrated an increase in damage, with a low of 21.29% DNA in the tail for the 0 μM bleomycin, a slight increase in damage for transfected cells with 0 μM bleomycin at 25.03% DNA in the tail, then progressively increasing damage for increasing treatment concentrations. Damage for cells exposed to 0-0.01 μM bleomycin is less than that measured in control untransfected cells, while damage for 0.1 and 1 μM treatments is higher than untransfected cells. In transfected cells there was 56.34% and 66.62% DNA in the tail for 0.1 and 1 μM respectively compared to untransfected cells with 34.56% and 51.2% for the same concentrations. Unlike menadione treatment, HEK293T cells responded to the low dose concentrations of bleomycin from 0.001-10 μM with increasing damage, yet the low-efficiency transfection of FANCJ still seemed to have a protective effect for cells treated with 0-0.01 μM bleomycin. Transfected cells exposed to 0.1 and 1 μM bleomycin, however, exhibited higher damage compared to the untransfected controls. It is possible that lower concentrations of treatment induce damage repair pathways like with menadione treatment. At higher bleomycin treatment concentrations, however, low-efficiency FANCJ transfection seems to increase damage susceptibility of HEK293T cells.

For the cells imaged using DAPI, there was a lower level of baseline damage consistent to the overall lower baseline seen for menadione-treated cells imaged with DAPI. The untransfected control cells demonstrated increasing damage for increasing bleomycin except at the lowest treatment concentration of 0.001 μM with 10.62% DNA

in the comet tail, which was slightly lower than cells with 0 μM treatment and a baseline damage of 11.34% DNA in the tail. An increase in damage was seen for increasing treatment concentrations with 0.01 μM at 12.18%, 0.1 μM at 13.51%, 1 μM at 24.43%, and 10 μM at 54.77% DNA in the tail. Cells transfected with FANCJ-mNG also demonstrated increasing damage with increasing treatment concentration. Unlike the low-efficiency FANCJ transfection, the 20% efficiency transfection of FANCJ-mNG did not cause a protective effect for the lowest concentrations of bleomycin treatments. Instead, a slight decrease in damage was seen for 1 μM bleomycin with 21.97% DNA in the tail for transfected cells compared to 24.43% in untransfected cells. For all other treatment concentrations, untransfected cells and cells transfected with FANCJ-mNG had roughly the same amount of damage accumulation. This differs from the low-efficiency transfection of FANCJ, which had increased damage at higher bleomycin concentrations. The difference seen between the 4% and 20% transfections at the higher bleomycin treatments may indicate that FANCJ overexpression was able to suppress damage that the low-efficiency transfection seemed to induce.

Overall, these assays again demonstrate the high sensitivity of SYBR Gold stain and the subsequent increase in data variability. HEK293T cells exposed to 0.001-10 μM bleomycin demonstrated increasing damage accumulation with both SYBR Gold and DAPI staining. The data suggests that the transfection of FANCJ-EBFP2 with a low level of efficiency may aid in the suppression of DNA damage at low concentrations of bleomycin from 0-0.01 μM. Conversely, at higher concentrations of bleomycin at 0.1-1 μM, the transfection of FANCJ-EBFP2 may have hindered DNA repair or compounded upon DNA damage caused by bleomycin. Higher FANCJ transfection efficiency with the

FANCJ-mNG construct may have improved cell viability at higher concentrations of bleomycin demonstrated by the comparable damage for untransfected and transfected cells at 0.1, 1, and 10 μM treatments opposed to the increase in damage seen between transfected and untransfected cells seen for FANCJ-EBFP2. These results show that damage from low bleomycin treatment concentrations may be suppressed by the triggering of endogenous DNA repair pathways, while higher treatments may require the support of repair protein overexpression to suppress DNA damage accumulation.

Bleomycin (μM)	% DNA in Tail Control (SYBR Gold)	% DNA in Tail FANCJ-EBFP2 (SYBR Gold)	% DNA in Tail Control (DAPI)	% DNA in Tail FANCJ-mNG (DAPI)
0 (No FANCJ)	34.94 ± 18.82	21.29 ± 14.74	11.34 ± 2.82	10.60 ± 0.64
0	-	25.03 ± 15.33	-	10.67± 0.99
0.001	37.11 ± 20.49	32.47 ± 13.49	10.62 ± 1.79	11.36 ± 0.01
0.01	41.11 ± 20.75	40.22 ± 24.73	12.18 ± 1.75	11.21 ± 1.71
0.1	34.56 ± 12.77	56.34 ± 40.19	13.51 ± 2.82	13.57 ± 1.64
1	51.52 ± 21.94	66.62 ± 37.18	24.43 ± 3.27	21.97 ± 6.30
10	64.26 ± 13.91	-	54.77 ± 13.99	54.56 ± 1.22

Table 3.2: Damage results for HEK293T cells with bleomycin: The percent DNA in the comet tail is used to determine the extent of DNA damage of cells transfected with either FANCJ-EBFP2 (4% transfection efficiency) or FANCJ-mNG (20% transfection efficiency) compared to untransfected controls.

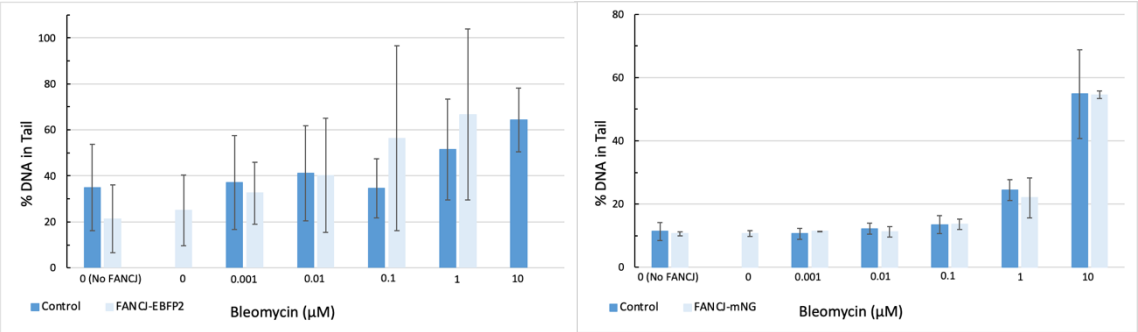

Figure 3.4: HEK293T cells with bleomycin treatment: The graph on the left depicts the untransfected control cells compared to FANCJ-EBFP2 transfected cells exposed to 0, 0.001, 0.01, 0.1, 1, and 10 µM bleomycin. These cells were imaged using SYBR Gold stain. The graph on the right depicts the untransfected control cells compared to FANCJ-mNG transfected cells exposed to the same concentrations of bleomycin. These cells were imaged using DAPI stain. For both conditions, a general increase in damage is seen as bleomycin concentrations increase. While the transfection of FANCJ-EBFP2 either suppressed or exacerbated damage induction, the transfection of FANCJ-mNG shows similar or decreased damage compared to control cells.

3.3.3 Conclusions

Alkaline comet assays were performed on HEK293T cells treated with varying concentrations of menadione or bleomycin and transfected with either FANCJ-EBFP2 with a low transfection efficiency of 4% or FANCJ-mNG with a higher transfection efficiency of 20%. The results demonstrate that low concentrations of menadione treatment at 0.001-10 µM do not cause significant levels of DNA damage, and that transfection can improve damage tolerance in these. Both low concentrations of

menadione and transfection reagents may trigger DNA damage response pathways to suppress damage accumulation.

Bleomycin-treated cells showed a more robust damage profile in response to increasing treatment concentrations. Cells transfected with FANCJ-EBFP2 with a 4% efficiency exhibited a protective effect at treatment concentrations of 0.001-0.1 μM but had heightened damage accumulation at 1 and 10 μM. Cells transfected with FANCJ-mNG with 20% efficiency demonstrated a similar damage profile to untransfected cells, suggesting that the overexpression of FANCJ may have been able to suppress damage induced by transfection reagents. Compared to menadione, endogenous DNA damage response systems triggered by bleomycin or transfection reagents may not be sufficient to suppress damage accumulation, but FANCJ overexpression may improve outcomes.

3.4 Discussion and Future Directions

DNA damage suppression is essential to maintain genomic stability and promote cell survival. When DNA repair proteins are downregulated in healthy cells, DNA mutations and damage accumulate, often leading to cancerous growth or cell death [17, 19, 62]. Antitumoral drugs often target DNA to induce damage and trigger cell senescence or apoptosis [74, 77, 78, 84]. In cancer cells, the overexpression of DNA repair proteins aids in cancer cell survival by repairing chemotherapeutic induced damage [2, 4, 32]. Discovering the mechanisms behind cancer cell evasion of chemotherapeutic drugs is an important endeavor to improve treatment outcomes. Additionally, understanding the response of healthy cells exposed to the same chemotherapeutic drugs will help to uncover more about DNA damage response pathways, the potential for cancer prevention, and how to better protect non-cancerous cells during cancer treatment.

In this study, we have begun to investigate the effects of low concentrations of the DNA damage inducers menadione and bleomycin on non-cancerous HEK293T cells with upregulation of the DNA damage repair protein FANCJ. This investigation helps determine the cellular response for natural damage suppression at treatment conditions that are low enough to cause DNA damage, but not cell death. The overexpression of FANCJ helps illuminate the potential for DNA damage repair protein upregulation to have a protective effect in healthy cells similar to that observed in cancerous cells. In healthy cells, repair protein upregulation may serve to improve cell survival during chemotherapeutic treatments and prevent mutagenesis that leads to cancerous growth.

We used alkaline comet assays to measure DNA damage accumulation in cells treated with 0.001-10 μM menadione or bleomycin with the FA repair protein FANCJ transfected with low or higher efficiency. Our results suggest that menadione concentrations ranging from 0.001-10 μM are too low to cause considerable DNA damage, however, are high enough to activate DNA repair pathways. This was observed by the relative decrease in DNA damage of cells treated with menadione compared to untreated controls. Additionally, both the 4% and 20% efficiency transfections of FANCJ further suppressed DNA damage. Because this occurred for both low and higher FANCJ upregulation, it is likely that the process of transfection alone was sufficient to initiate repair mechanisms within the cell, rather than damage suppression by the transfected FANCJ. For Bleomycin, the treatment concentrations were sufficient to elevate DNA damage, which increased corresponding to increasing treatment concentrations. Low-efficiency transfection seemed to have a protective effect for cells exposed to 0.001-0.01 μM bleomycin, while it exacerbated damage accumulation for 0.1 and 1 μM treatments.

The higher-efficiency transfection yielded results very similar to untreated cells. For 1 and 10 μM, the higher-efficiency FANCJ transfection had a slight protective effect compared to untreated cells and low-efficiency transfected cells. It is likely that the overexpression of FANCJ was capable of suppressing DNA damage by bleomycin at these concentrations.

Overall, our results suggest that very low concentrations of the damage inducers menadione and bleomycin are able to activate DNA repair mechanisms, and that transfection reagents may do the same. While FANCJ overexpression seems to supress damage at higher concentrations of bleomycin, the transfection process may make cells more vulnerable to higher concentrations of menadione. These results are limited by the concentration ranges of the two damage inducers. Future experiments will expand these concentration ranges above 10 μM. Additionally, results from alkaline comet assays measuring ssDNA and dsDNA breaks can be supported by the use of neutral assays to assess primarily dsDNA breaks [84]. Alternative detection methods could also be used, including ROS measurements for menadione treatment utilizing the fluorescent probes 5-(6)-carboxy-2′,7′-dichlorodihydrofluorescein diacetate (DCFDA) to quantify intracellular ROS in response to increasing treatment concentrations [85]. DNA damage could then be compared to ROS levels rather than to menadione concentration alone. For a real time analysis of DNA damage, a novel engineered chromatin reader biomarker for dsDNA breaks could be used [86]. The probe binds to a biomarker of dsDNA breaks known as γ-H2AX and allows the fluorescent tracking of break formation and repair when viewed under confocal microscopy [86]. Using this probe, DNA damage could be measured via fluorescent puncta quantification in cells exposed to damage inducers. This would allow

for real time analysis of damage induction and would enable fluorescently labeled proteins such as our FANCJ-EBFP2 or FANCJ-mNG to be localized to damage sites during DNA repair. These studies would provide valuable information to better understand DNA damage repair protein localization and repair kinetics.

Our lab would also like to expand upon damage suppression experiments by investigating the effects of upregulating the full length REV1 and FANCJ proteins independently and together in cells exposed to G4 stabilizers. The *in vivo* experimentation with these proteins would support current research to provide valuable information about REV1 and FANCJ in G4 unfolding and overall damage accumulation or suppression when G4s are stabilized. Due to the low transfection efficiency seen with our FANCJ constructs, we would also like to utilize the Fluorescence Activated Cell Sorting (FACS) Aria instrument to isolate fluorescently labeled transfected cells for experimentation [87]. This would ensure that untransfected cells are not present and that changes in damage profiles are the result of upregulated protein and not solely from exposure to transfection reagents.

Moving forward with damage assessment experiments, we intend to investigate the roles of REV1 and FANCJ in damage suppression of cells exposed to damage inducers and G4 stabilizers. This research will continue to build upon current knowledge of DNA damage repair proteins, their interactions, and their abilities to promote genomic stability.

CHAPTER FOUR

CONCLUSIONS AND FUTURE DIRECTIONS

4.0 Conclusions

The purpose of this study was to expand the understanding of the TLS repair pathway protein REV1 polymerase and FA repair pathway protein FANCJ helicase in their roles of G4 unwinding and DNA damage suppression. We sought to determine why two proteins from different repair pathways might have the same abilities to unfold G4 DNA outside of their normal pathway functions. We suspected that REV1 and FANCJ would exhibit a complementary role in G4 unfolding by preferentially targeting different G4 conformations. Additionally, we examined the ability of FANCJ upregulation to suppress DNA damage induced by low concentrations of menadione or bleomycin. We expected that increasing treatment concentrations would generate more DNA damage in cells, and that FANCJ upregulation would help to suppress this damage. These studies seek to understand the roles of REV1 and FANCJ in maintaining genomic stability at G4 sites or damaged DNA.

Our unfolding experiments demonstrated that REV1 and FANCJ were capable of effectively unfolding both the hybrid $(TTAGGG)_4$ and parallel $(GGGT)_4$ G4 constructs with and without oxidative damage. REV1 unfolded the hybrid sequence with and without damage with a higher efficiency than the parallel sequence and a higher efficiency compared to FANCJ unfolding the hybrid G4. FANCJ unfolded both conformations with similar efficiencies, yet FANCJ unfolded the parallel structure with a higher efficiency than REV1. These results suggest that REV1 preferentially unfolds

hybrid sequences, while FANCJ can unfold either conformation but may preferentially target parallel sequences that REV1 cannot unfold as readily. This would demonstrate a complementary role in G4 unfolding, that helps to explain why both proteins are essential in maintaining genomic stability at G4 sites. Additionally, neither protein required ATP for G4 unfolding. It is likely that protein binding is sufficient for initial disruption of the G4 structure, and that after REV1 or FANCJ bind and unfold the G4, additional pols are recruited to replicate the relaxed structure.

The results of our DNA damage experiments show that menadione concentrations from 0.001-10 μM do not cause significant DNA damage accumulation in HEK293T cells after a two-hour incubation. Instead, these concentrations may be enough to trigger DNA damage response pathways which suppressed any treatment induced damage and repaired even baseline levels of damage. Conversely, the same concentrations of bleomycin induced measurable changes in DNA damage. Low-efficiency transfection of FANCJ further complimented the endogenous repair pathway response in menadione-treated cells, as damage was suppressed more than untransfected cells. For bleomycin-treated cells, this response was seen for 0.001 and 0.01 μM, but low transfection efficiency of FANCJ seemed to increase damage susceptibility at 0.1 and 1 μM treatments. The higher-efficiency transfection of FANCJ exhibited the same damage suppression response in menadione-treated cells as the low-efficiency transfection. Transfected cells treated with menadione had lower damage accumulation compared to untransfected cells and even the untreated control. For bleomycin-treated cells, higher-efficiency FANCJ transfection yielded similar damage profiles to untransfected cells. At 1 and 10 μM bleomycin, FANCJ overexpression slightly suppressed damage

accumulation, both compared to low-efficiency transfection and untransfected cells. Overall, these results suggest that at low enough concentrations, damage inducers can stimulate DNA damage repair mechanisms and suppress damage accumulation even below the baseline damage of untreated cells. Additionally, the transfection process may have a similar effect in stimulating natural DNA damage repair in cells exposed to low treatment concentrations, but may exacerbate damage once concentrations rise. Upregulation of the FA repair protein FANCJ likely has a protective effect for cells exposed to higher concentrations of bleomycin, however further investigation is necessary to examine the effects of upregulation at treatment concentrations above 10 μM.

Overall, these results propose a model of G4 unfolding where FANCJ binds and unfolds parallel sequences then recruits REV1 or additional TLS pols to replicate the DNA, while REV1 can bind and unfold hybrid G4s before replicating the DNA or recruiting additional pols. This process is not hindered by oxidative damage. Additionally, cells exposed to damage inducers at low concentrations exhibit a natural damage suppression response, likely from the activation of DNA damage repair pathways. The upregulation of FANCJ may suppress damage accumulation in noncancerous cells exposed to bleomycin.

4.1 Future Directions

The continued research of repair pathway proteins is essential to the development of new and targeted cancer treatments. Expanding upon our current research we would like to continue the investigation of REV1 and FANCJ in their roles of G4 unfolding using a direct biophysical approach to examine the mechanism of unfolding for

either protein independently as well as the interaction during unfolding when the two proteins are together. We would like to expand the G4 constructs used to include additional parallel and hybrid forming sequences as well as anti-parallel G4s to gain a more generalized view of REV1 and FANCJ specificity for these constructs.

As we move forward with DNA damage experiments, we seek to isolate successfully transfected cells to examine the effects of upregulation without conflicting data from cells that do not exhibit protein upregulation. We also aim to transfect the full length REV1 into cells both independently and in conjunction with FANCJ to examine the ability of these proteins to suppress damage accumulation. Investigating the effects of REV1 and FANCJ upregulation in cells exposed to G4 stabilizers will improve the understanding of the *in vivo* effects of these proteins in overall G4 maintenance.

REV1 and FANCJ are known proteins necessary for DNA damage repair and G4 maintenance [36, 37, 38, 55]. Both G4s and repair proteins have already exhibited their potential as therapeutic targets to suppress cancer formation and proliferation [47, 48, 49, 62]. As scientists continue to investigate the roles that REV1, FANCJ, and other DNA repair proteins play in damage repair both within and outside of typical repair pathways, these discoveries will pave the way for new targeted cancer therapies.

APPENDIX

IBC APPROVAL LETTER

cayuse Hazard Safety

Reference: IBC Protocol # IBC-00001119

Protocol Title: Mutational analysis of DNA repair proteins

Principal Investigator: Wu, Colin

Approval Period: 02/20/2024 - 02/20/2027

Dear Professor Wu, Colin:
The Institutional Biosafety Committee (IBC), responsible for the review of research involving materials of human origin, recombinant DNA, and biohazardous, infectious or toxic materials, has reviewed the original proposal, noted the revisions provided by you upon committee's request (if applicable), and approved the project referenced above. This is your formal approval notice; please save it for your records.

The proposed activities are approved for a period of three years, starting 02/20/2024 and ending 02/20/2027, and assigned the approval # IBC-00001119. Please be aware that protocols expire at 12:01 AM on the expiration date. The highest BSL level approved for the protocol can be found on the Overview page of the protocol form.

Any unanticipated problems, changes in, or halting of the activities proposed in the project, as described, must be promptly reported to the IBC or the biosafety officer.

In addition, all faculty, staff, and students involved in the project must be trained and qualified to conduct the project in a responsible manner. Please note, in this regard, that you, the Principal Investigator, are fully responsible at all times for limiting or restricting access to laboratories and for assessing, in each circumstance, who may enter or work in a laboratory when biohazardous materials are in use.

Prior to initiating any work on this approved project, please contact me by email (jdhallau@oakland.edu) to schedule a startup Biosafety Audit. This audit will verify that all biosafety controls described in your application have been implemented.

Please let me know if you have any questions. Thank you.

Sincerely,

Janell Hallauer
Biosafety Officer
Laboratory Safety and Compliance

REFERENCES

1. Khatib, J. B., Nicolae, C. M., & Moldovan, G.-L. (2023). Role of Translesion DNA Synthesis in the Metabolism of Replication-associated Nascent Strand Gaps. *Journal of Molecular Biology*, *436*(1), 168275. https://doi.org/10.1016/j.jmb.2023.168275
2. Ler, A. A. L., & Carty, M. P. (2022). DNA Damage Tolerance Pathways in Human Cells: A Potential Therapeutic Target. *Frontiers in Oncology*, https://doi.org/10.3389/fonc.2021.822500
3. Goodman, M. F., & Woodgate, R. (2013). Translesion DNA Polymerases. *Cold Spring Harbor Perspectives in Biology*, *5*(10), a010363–a010363. https://doi.org/10.1101/cshperspect.a010363
4. Yamanaka, K., Chatterjee, N., Hemann, M. T., & Walker, G. C. (2017). Inhibition of mutagenic translesion synthesis: A possible strategy for improving chemotherapy? *PLOS Genetics*, *13*(8), e1006842. https://doi.org/10.1371/journal.pgen.1006842
5. Estep, K. N., Butler, T. J., Ding, J., & Brosh, R. M. (2019). G4-Interacting DNA Helicases and Polymerases: Potential Therapeutic Targets. *Current Medicinal Chemistry*, *26*(16), 2881–2897. https://doi.org/10.2174/0929867324666171116123345
6. Nair, D. T. (2005). Rev1 Employs a Novel Mechanism of DNA Synthesis Using a Protein Template. *Science*, *309*(5744), 2219–2222. https://doi.org/10.1126/science.1116336

7. Weaver, T. M., Click, T. H., Khoang, T. H., Todd Washington, M., Agarwal, P. K., & Freudenthal, B. D. (2022). Mechanism of nucleotide discrimination by the translesion synthesis polymerase Rev1. *Nature Communications*, *13*(1), 2876.
8. Weaver, T. M., Cortez, L. M., Khoang, T. H., Washington, M. T., Agarwal, P. K., & Freudenthal, B. D. (2020). Visualizing Rev1 catalyze protein-template DNA synthesis. *Proceedings of the National Academy of Sciences*, *117*(41), 25494–25504. https://doi.org/10.1073/pnas.2010484117
9. Nair, D. T., Johnson, R. E., Prakash, L., Prakash, S., & Aggarwal, A. K. (2010). DNA Synthesis across an Abasic Lesion by Yeast Rev1 DNA Polymerase. *Journal of Molecular Biology*, *406*(1), 18–28. https://doi.org/10.1016/j.jmb.2010.12.016
10. Pustovalova, Y., Bezsonova, I., & Korzhnev, D. M. (2012). The C-terminal domain of human Rev1 contains independent binding sites for DNA polymerase η and Rev7 subunit of polymerase ζ. *FEBS Letters*, *586*(19), 3051–3056. https://doi.org/10.1016/j.febslet.2012.07.021
11. Barnes, R. P., Tsao, W.-C., Moldovan, G.-L., & Eckert, K. A. (2018). DNA Polymerase Eta Prevents Tumor Cell-Cycle Arrest and Cell Death during Recovery from Replication Stress. *Cancer Research*, *78*(23), 6549–6560. https://doi.org/10.1158/0008-5472.can-17-3931
12. Rodriguez, G. P., Song, J. B., & Crouse, G. F. (2013). In Vivo Bypass of 8-oxodG. *PLoS Genetics*, *9*(8), e1003682. https://doi.org/10.1371/journal.pgen.1003682

13. van der Sluijs, R. V., Verkennis, A. E. E., Hodskinson, M. R., Barnett, J., Cruz, V. M., Hernandez-Quiles, M., Liolios, T., Morton, S. B., Hendrikx, A., Bos, C., Post, H., Millington, C. L., Rouillon, C., Ricci, G., Mattiroli, F., Williams, D. M., Altelaar, M., Vermeulen, M., Patel, K. J., & Knipscheer, P. (2025). DNA polymerase kappa is the primary translesion synthesis polymerase for aldehyde ICLs. *Nucleic acids research*, *53*(18), gkaf875. https://doi.org/10.1093/nar/gkaf875
14. Du, H., Wang, P., Li, L., & Wang, Y. (2019). *Repair and translesion synthesis of O6-alkylguanine DNA lesions in human cells*. *294*(29), 11144–11153. https://doi.org/10.1074/jbc.ra119.009054
15. Albertella, M. R., Lau, A., & O'Connor, M. J. (2005). The overexpression of specialized DNA polymerases in cancer. *DNA Repair*, *4*(5), 583–593. https://doi.org/10.1016/j.dnarep.2005.01.005
16. Nayak, S., Calvo, J. A., & Cantor, S. B. (2021). Targeting translesion synthesis (TLS) to expose replication gaps, a unique cancer vulnerability. *Expert Opinion on Therapeutic Targets*, *25*(1), 27–36. https://doi.org/10.1080/14728222.2021.1864321
17. *The Fanconi Anemia DNA Repair Pathway*. (n.d.). Fanconi Cancer Foundation. https://fanconi.org/clinical-care-guidelines/the-fanconi-anemia-dna-repair-pathway/
18. Brosh, R. M., Bellani, M., Liu, Y., & Seidman, M. M. (2017). Fanconi Anemia: A DNA repair disorder characterized by accelerated decline of the hematopoietic

stem cell compartment and other features of aging. *Ageing Research Reviews*, *33*, 67–75. https://doi.org/10.1016/j.arr.2016.05.005

19. Renaudin, X., Ahmad, A., Mancini, B., Gueiderikh, A., Noémie Louis-Joseph, Frédérique Maczkowiak-Chartois, & Rosselli, F. (2024). Contribution of p53-dependent and -independent mechanisms to upregulation of p21 in Fanconi anemia. *PLoS Genetics*, *20*(11), e1011474–e1011474. https://doi.org/10.1371/journal.pgen.1011474
20. Ishiai, M. (2021). Regulation of the Fanconi Anemia DNA Repair Pathway by Phosphorylation and Monoubiquitination. *Genes*, *12*(11), 1763. https://doi.org/10.3390/genes12111763
21. Lemonidis, K., Arkinson, C., Rennie, M. L., & Walden, H. (2021). Mechanism, specificity, and function of FANCD2-FANCI ubiquitination and deubiquitination. *The FEBS Journal*. https://doi.org/10.1111/febs.16077
22. Alcón, P., Kaczmarczyk, A. P., Ray, K. K., Liolios, T., Guilbaud, G., Sijacki, T., Shen, Y., McLaughlin, S. H., Sale, J. E., Knipscheer, P., Rueda, D. S., & Passmore, L. A. (2024). FANCD2–FANCI surveys DNA and recognizes double- to single-stranded junctions. *Nature*, 1–9. https://doi.org/10.1038/s41586-024-07770-w
23. Cole, A. R., Lewis, L. P. C., & Walden, H. (2010). The structure of the catalytic subunit FANCL of the Fanconi anemia core complex. *Nature Structural & Molecular Biology*, *17*(3), 294–298. https://doi.org/10.1038/nsmb.1759
24. Wu, Y., & Brosh Jr., R. (2009). FANCJ Helicase Operates in the Fanconi Anemia DNA Repair Pathway and the Response to Replicational Stress. *Current*

Molecular Medicine, *9*(4), 470–482. https://doi.org/10.2174/156652409788167159

25. Bharti, S. K., Sommers, J. A., Awate, S., Bellani, M. A., Khan, I., Bradley, L., King, G. A., Seol, Y., Vidhyasagar, V., Wu, Y., Abe, T., Kobayashi, K., Shin-ya, K., Kitao, H., Wold, M. S., Branzei, D., Neuman, K. C., & Brosh, R. M. (2018). A minimal threshold of FANCJ helicase activity is required for its response to replication stress or double-strand break repair. *Nucleic Acids Research*, *46*(12), 6238–6256. https://doi.org/10.1093/nar/gky403
26. Cantor, S. B., Bell, D. W., Ganesan, S., Kass, E. M., Drapkin, R., Grossman, S. R., Doke C.R. Wahrer, Sgroi, D. C., Lane, W. S., Haber, D. A., & Livingston, D. M. (2001). BACH1, a Novel Helicase-like Protein, Interacts Directly with BRCA1 and Contributes to Its DNA Repair Function. *Cell*, *105*(1), 149–160. https://doi.org/10.1016/s0092-8674(01)00304-x
27. Seal, S., Thompson, D., Renwick, A., Elliott, A., Kelly, P., Barfoot, R., Chagtai, T., Jayatilake, H., Ahmed, M., Spanova, K., North, B., McGuffog, L., Evans, D. G., Eccles, D., Easton, D. F., Stratton, M. R., & Rahman, N. (2006). Truncating mutations in the Fanconi anemia J gene BRIP1 are low-penetrance breast cancer susceptibility alleles. *Nature Genetics*, *38*(11), 1239–1241. https://doi.org/10.1038/ng1902
28. Zhang, F., Fan, Q., Ren, K., Auerbach, A. D., & Andreassen, P. R. (2010). FANCJ/BRIP1 recruitment and regulation of FANCD2 in DNA damage responses. *Chromosoma*, *119*(6), 637–649. https://doi.org/10.1007/s00412-010-0285-6

29. Chen, X., Wilson, J. B., McChesney, P. A., Williams, S., Kwon, Y., Longerich, S., Marriott, A., Sung, P., Jones, N. J., & Kupfer, G. M. (2014). *The Fanconi Anemia Proteins FANCD2 and FANCJ Interact and Regulate Each Other's Chromatin Localization*. *289*(37), 25774–25782. https://doi.org/10.1074/jbc.m114.552570

30. Odermatt, D. C., Ting, W., Wild, S., Jozwiakowski, S. K., Rothenberg, E., & Gari, K. (2020). Cancer-associated mutations in the iron-sulfur domain of FANCJ affect G-quadruplex metabolism. *PLoS Genetics*, *16*(6), e1008740–e1008740. https://doi.org/10.1371/journal.pgen.1008740

31. Brosh, R. M., & Cantor, S. B. (2014). Molecular and cellular functions of the FANCJ DNA helicase defective in cancer and in Fanconi anemia. *Frontiers in Genetics*, *5*. https://doi.org/10.3389/fgene.2014.00372

32. Kao, W. H., Riker, A. I., Kushwaha, D. S., Ng, K., Enkemann, S. A., Jove, R., Buettner, R., Zinn, P. O., Sánchez, N. P., Villa, J. L., D'Andrea, A. D., Sánchez, J. L., Kennedy, R. D., Chen, C. C., & Matta, J. L. (2011). Upregulation of Fanconi Anemia DNA Repair Genes in Melanoma Compared with Non-Melanoma Skin Cancer. *Journal of Investigative Dermatology*, *131*(10), 2139–2142. https://doi.org/10.1038/jid.2011.181

33. Yang, Y., Liu, Z., Wang, F., Piya Temviriyanukul, Ma, X., Tu, Y., Lingna Lv, Lin, Y.-F., Huang, M., Zhang, T., Pei, H., Chen, B. P. C., Jansen, J. G., Wind, N. de, Fischhaber, P. L., Friedberg, E. C., Tang, T.-S., & Guo, C. (2015). FANCD2 and REV1 cooperate in the protection of nascent DNA strands in response to

replication stress. *Nucleic Acids Research*, *43*(17), 8325–8339. https://doi.org/10.1093/nar/gkv737

34. de Krijger, I., Boersma, V., & Jacobs, J. J. L. (2021). REV7: Jack of many trades. *Trends in Cell Biology*, *31*(8), 686–701. https://doi.org/10.1016/j.tcb.2021.04.002
35. Lowran, K., Campbell, L., Popp, P., & Wu, C. (2019). *Assembly of a G-Quadruplex Repair Complex by the FANCJ DNA Helicase and the REV1 Polymerase*. https://doi.org/10.3390/genes11010005
36. Sarkies, P., Murat, P., Phillips, L. G., Patel, K. J., Balasubramanian, S., & Sale, J. E. (2011). FANCJ coordinates two pathways that maintain epigenetic stability at G-quadruplex DNA. *Nucleic Acids Research*, *40*(4), 1485–1498. https://doi.org/10.1093/nar/gkr868
37. Ketkar, A., Smith, L., Johnson, C., Richey, A., Berry, M., Hartman, J. H., Maddukuri, L., Reed, M. R., Gunderson, J., Leung, J., & Eoff, R. L. (2021). Human Rev1 relies on insert-2 to promote selective binding and accurate replication of stabilized G-quadruplex motifs. *Nucleic Acids Research*, *49*(4), 2065–2084. https://doi.org/10.1093/nar/gkab041
38. Eddy, S., Amit Ketkar, Zafar, M. K., Maddukuri, L., Choi, J.-Y., & Eoff, R. L. (2013). Human Rev1 polymerase disrupts G-quadruplex DNA. *Nucleic Acids Research*, *42*(5), 3272–3285. https://doi.org/10.1093/nar/gkt1314
39. Varshney, D., Spiegel, J., Zyner, K., Tannahill, D., & Balasubramanian, S. (2020). The regulation and functions of DNA and RNA G-quadruplexes. *Nature Reviews Molecular Cell Biology*, *21*. https://doi.org/10.1038/s41580-020-0236-x

40. Hänsel-Hertsch, R., Beraldi, D., Lensing, S. V., Marsico, G., Zyner, K., Parry, A., Di Antonio, M., Pike, J., Kimura, H., Narita, M., Tannahill, D., & Balasubramanian, S. (2016). G-quadruplex structures mark human regulatory chromatin. *Nature Genetics*, *48*(10), 1267–1272. https://doi.org/10.1038/ng.3662

41. Hao, F., Ma, Y., & Guan, Y. (2019). Effects of Central Loop Length and Metal Ions on the Thermal Stability of G-Quadruplexes. *Molecules*, *24*(10), 1863. https://doi.org/10.3390/molecules24101863

42. Burge, S., Parkinson, G. N., Hazel, P., Todd, A. K., & Neidle, S. (2006). Quadruplex DNA: sequence, topology and structure. *Nucleic Acids Research*, *34*(19), 5402–5415. https://doi.org/10.1093/nar/gkl655

43. Meier-Stephenson, V. (2022). G4-quadruplex-binding proteins: review and insights into selectivity. *Biophysical Reviews*, *14*(3), 635–654. https://doi.org/10.1007/s12551-022-00952-8

44. Rodriguez, G. P., Song, J. B., & Crouse, G. F. (2013). In Vivo Bypass of 8-oxodG. *PLoS Genetics*, *9*(8), e1003682. https://doi.org/10.1371/journal.pgen.1003682

45. Gorini, F., Ambrosio, S., Lania, L., Majello, B., & Amente, S. (2023). The Intertwined Role of 8-oxodG and G4 in Transcription Regulation. *International Journal of Molecular Sciences*, *24*(3), 2031. https://doi.org/10.3390/ijms24032031

46. Teng, F.-Y., Jiang, Z.-Z., Guo, M., Tan, X.-Z., Chen, F., Xi, X.-G., & Xu, Y. (2021). G-quadruplex DNA: a novel target for drug design. *Cellular and*

Molecular Life Sciences, *78*(19-20), 6557–6583. https://doi.org/10.1007/s00018-021-03921-8

47. Iachettini, S., Biroccio, A., & Zizza, P. (2024). Therapeutic Use of G4-Ligands in Cancer: State-of-the-Art and Future Perspectives. *Pharmaceuticals*, *17*(6), 771–771. https://doi.org/10.3390/ph17060771
48. Lin, J., Gong, Z., Lu, Y., Cai, J., Zhang, J., Tan, J., Huang, Z., & Chen, S. (2025). Recent Progress and Potential of G4 Ligands in Cancer Immunotherapy. *Molecules*, *30*(8), 1805–1805. https://doi.org/10.3390/molecules30081805
49. Yang, Q.-F., Wang, X.-R., Wang, Y.-H., Wu, X.-H., Shi, R.-Y., Wang, Y.-X., Zhu, H.-N., Yang, S., Tang, Y.-L., & Li, F. (2024). G4LDB 3.0: a database for discovering and studying G-quadruplex and i-motif ligands. *Nucleic Acids Research*. https://doi.org/10.1093/nar/gkae835
50. Lowran, K. A. (2024). *Mechanisms of G-Quadruplex Recognition and Unfolding by the FANCJ Helicase and REV1 Polymerase.*
51. Rémy Bétous, Rey, L., Wang, G., Marie-Jeanne Pillaire, Puget, N., Janick Sèlves, Biard, D., Kazuo Shin-ya, Vásquez, K. M., Christophe Cazaux, & Hoffmann, J.-S. (2008). Role of TLS DNA polymerases eta and kappa in processing naturally occurring structured DNA in human cells. *Molecular Carcinogenesis*, *48*(4), 369–378. https://doi.org/10.1002/mc.20509
52. Eddy, S., Tillman, M., Maddukuri, L., Ketkar, A., Zafar, M. K., & Eoff, R. L. (2016). Human Translesion Polymerase κ Exhibits Enhanced Activity and Reduced Fidelity Two Nucleotides from G-Quadruplex DNA. *Biochemistry*, *55*(37), 5218–5229. https://doi.org/10.1021/acs.biochem.6b00374

53. Bedaiwi, S., Usmani, A., & Carty, M. P. (2024). Canonical and Non-Canonical Roles of Human DNA Polymerase η. *Genes*, *15*(10), 1271. https://doi.org/10.3390/genes15101271

54. Edmunds, C. E., Simpson, L. J., & Sale, J. E. (2008). *PCNA Ubiquitination and REV1 Define Temporally Distinct Mechanisms for Controlling Translesion Synthesis in the Avian Cell Line DT40*. *30*(4), 519–529. https://doi.org/10.1016/j.molcel.2008.03.024

55. Sarkies, P., Reams, C., Simpson, L. J., & Sale, J. E. (2010). Epigenetic Instability due to Defective Replication of Structured DNA. *Molecular Cell*, *40*(5), 703–713. https://doi.org/10.1016/j.molcel.2010.11.009

56. Siegel, A., Almstead, D., Naveen Kothandaraman, Reich, J., Lamkin, E., Victor, J., Grover, A., Kanayo Ikeh, Koval, H., Crompton, A., Jang, H., Lee, H., Del, R., Dmitry Korzhnev, Hadden, M. K., Hong, J., Zhou, P., & Chatterjee, N. (2025). REV1 inhibition enhances trinucleotide repeat mutagenesis. *BioRxiv (Cold Spring Harbor Laboratory)*. https://doi.org/10.1101/2025.09.11.675234

57. CDC. *Cancer Data and Statistics*. Cancer. https://www.cdc.gov/cancer/data/index.html.

58. Zhang, H., Zhou, J., & Ye, Y. (2024). Prediction and validation of circulating G-quadruplexes as a novel biomarker in colorectal cancer. *Journal of Gastrointestinal Oncology*, *15*(1). https://doi.org/10.21037/jgo-24-26

59. Robinson, N. J., & Schiemann, W. P. (2022). Telomerase in Cancer: Function, Regulation, and Clinical Translation. *Cancers*, *14*(3), 808. https://doi.org/10.3390/cancers14030808

60. Figueiredo, J., Mergny, J.-L., & Cruz, C. (2024). G-quadruplex ligands in cancer therapy: Progress, challenges, and clinical perspectives. *Life Sciences*, *340*, 122481. https://doi.org/10.1016/j.lfs.2024.122481

61. Grand, C. L., Han, H., Muñoz, R. M., Weitman, S., Von, D. D., Hurley, L. H., & Bearss, D. J. (2002). The cationic porphyrin TMPyP4 down-regulates c-MYC and human telomerase reverse transcriptase expression and inhibits tumor growth in vivo. *PubMed*, *1*(8), 565–573.

62. Chen, Y., Jie, X., Xing, B., Wu, Z., Yang, X., Rao, X., Xu, Y., Zhou, D., Dong, X., Zhang, T., Yang, K., Li, Z., & Wu, G. (2022). REV1 promotes lung tumorigenesis by activating the Rad18/SERTAD2 axis. *Cell Death & Disease*, *13*(2). https://doi.org/10.1038/s41419-022-04567-5

63. Wu, G., Tillo, D., Ray, S., Chang, T.-C., Schneekloth, J. S., Vinson, C., & Yang, D. (2020). Custom G4 Microarrays Reveal Selective G-Quadruplex Recognition of Small Molecule BMVC: A Large-Scale Assessment of Ligand Binding Selectivity. *Molecules*, *25*(15), 3465. https://doi.org/10.3390/molecules25153465

64. Chang, C.-C., Kuo, I.-C., Ling, I.-F., Chen, C.-T., Chen, H.-C., Lou, P.-J., Lin, J.-J., & Chang, T.-C. (2004). Detection of Quadruplex DNA Structures in Human Telomeres by a Fluorescent Carbazole Derivative. *Analytical Chemistry*, *76*(15), 4490–4494. https://doi.org/10.1021/ac049510s

65. Tseng, T.-Y., & Chang, T.-C. (2022). Imaging Study of Small Molecules to G-Quadruplexes in Cells. *Handbook of Chemical Biology of Nucleic Acids* , 1–38. https://doi.org/10.1007/978-981-16-1313-5_32-1

66. Lin, I., Tsai, Y., Kang, C., Huang, W., Wang, C., Lin, M., Lou, P., Shih, J., Wang, H., Wu, H., Tsai, T., Jan, I., & Chang, T. (2014). BMVC test, an improved fluorescence assay for detection of malignant pleural effusions. *Cancer Medicine*, *3*(1), 162–173. https://doi.org/10.1002/cam4.179

67. Nasab, M. G., Hassani, L., Nejad, S. M., & Davood Norouzi. (2016). Interaction of hemin with quadruplex DNA. *Journal of Biological Physics*, *43*(1), 5–14. https://doi.org/10.1007/s10867-016-9430-7

68. Lombardo, M. E., Araujo, L. S., Ciccarelli, A. B., & Batlle, A. (2004). A spectrophotometric method for estimating hemin in biological systems. *Analytical Biochemistry*, *341*(2), 199–203. https://doi.org/10.1016/j.ab.2004.11.002

69. Liu, H., Lu, Y.-N., Paul, T., Periz, G., Banco, M. T., Ferré-D'Amaré, A. R., Rothstein, J. D., Hayes, L. R., Myong, S., & Wang, J. (2021). A Helicase Unwinds Hexanucleotide Repeat RNA G-Quadruplexes and Facilitates Repeat-Associated Non-AUG Translation. *Journal of the American Chemical Society*, *143*(19), 7368–7379. https://doi.org/10.1021/jacs.1c00131

70. Cheng, Y., Zhang, Y., & You, H. (2021). Characterization of G-Quadruplexes Folding/Unfolding Dynamics and Interactions with Proteins from Single-Molecule Force Spectroscopy. *Biomolecules*, *11*(11), 1579. https://doi.org/10.3390/biom11111579

71. You, H., Lattmann, S., Rhodes, D., & Yan, J. (2016). RHAU helicase stabilizes G4 in its nucleotide-free state and destabilizes G4 upon ATP hydrolysis. *Nucleic Acids Research*, *45*(1), 206–214. https://doi.org/10.1093/nar/gkw881

72. Guo, L., Bao, Y., Zhao, Y., Ren, Z., Bi, L., Zhang, X., Liu, C., Hou, X., Wang, M. D., & Sun, B. (2023). Joint Efforts of Replicative Helicase and SSB Ensure Inherent Replicative Tolerance of G-Quadruplex. *Advanced Science*, *11*(9). https://doi.org/10.1002/advs.202307696

73. Loor, G., Kondapalli, J., Schriewer, J. M., Chandel, N. S., Vanden Hoek, T. L., & Schumacker, P. T. (2010). Menadione triggers cell death through ROS-dependent mechanisms involving PARP activation without requiring apoptosis. *Free Radical Biology and Medicine*, *49*(12), 1925–1936. https://doi.org/10.1016/j.freeradbiomed.2010.09.021

74. Morgan, W. A., Hartley, J. A., & Cohen, G. M. (1992). Quinone-induced DNA single strand breaks in rat hepatocytes and human chronic myelogenous leukaemic K562 cells. *Biochemical Pharmacology*, *44*(2), 215–221. https://doi.org/10.1016/0006-2952(92)90003-2

75. Kaźmierczak-Barańska, J., & Karwowski, B. T. (2022). Vitamin K Contribution to DNA Damage—Advantage or Disadvantage? A Human Health Response. *Nutrients*, *14*(20), 4219. https://doi.org/10.3390/nu14204219

76. Chen, J., Ghorai, M. K., Kenney, G., & Stubbe, J. (2008). Mechanistic studies on bleomycin-mediated DNA damage: multiple binding modes can result in double-stranded DNA cleavage. *Nucleic Acids Research*, *36*(11), 3781–3790. https://doi.org/10.1093/nar/gkn302

77. Chen, F., Zhao, W., Du, C., Chen, Z., Du, J., & Zhou, M. (2024). Bleomycin induces senescence and repression of DNA repair via downregulation of Rad51. *Molecular Medicine*, *30*(1). https://doi.org/10.1186/s10020-024-00821-y

78. Oztopcu-Vatan, P., Sayitoglu, M., Gunindi, M., & Inan, E. (2015). Cytotoxic and apoptotic effects of menadione on rat hepatocellular carcinoma cells. *Cytotechnology*, *67*(6), 1003–1009. https://doi.org/10.1007/s10616-014-9739-7

79. Clementi, E., Garajova, Z., & Markkanen, E. (2021). Measuring DNA Damage Using the Alkaline Comet Assay in Cultured Cells. *BIO-PROTOCOL*, *11*(16). https://doi.org/10.21769/bioprotoc.4119

80. Collins, A., Møller, P., Gajski, G., Vodenková, S., Abdulwahed, A., Anderson, D., Bankoglu, E. E., Bonassi, S., Boutet-Robinet, E., Brunborg, G., Chao, C., Cooke, M. S., Costa, C., Costa, S., Dhawan, A., de Lapuente, J., Bo', C. D., Dubus, J., Dusinska, M., & Duthie, S. J. (2023). Measuring DNA modifications with the comet assay: a compendium of protocols. *Nature Protocols*, *18*(3), 929–989. https://doi.org/10.1038/s41596-022-00754-y

81. *SYBR™ Gold Nucleic Acid Gel Stain (10,000X Concentrate in DMSO)*. (2022). Thermofisher.com. https://www.thermofisher.com/order/catalog/product/S11494

82. *DAPI (4',6-Diamidino-2-Phenylindole, Dihydrochloride)*. (2021). Thermofisher.com. https://www.thermofisher.com/order/catalog/product/D1306

83. Lorenzo, Y., Costa, S., Collins, A. R., & Azqueta, A. (2013). The comet assay, DNA damage, DNA repair and cytotoxicity: hedgehogs are not always dead. *Mutagenesis*, *28*(4), 427–432. https://doi.org/10.1093/mutage/get018

84. Figueroa-González, G., & Pérez-Plasencia, C. (2017). Strategies for the evaluation of DNA damage and repair mechanisms in cancer. *Oncology Letters*, *13*(6), 3982–3988. https://doi.org/10.3892/ol.2017.6002

85. Katerji, M., Filippova, M., & Duerksen-Hughes, P. (2019). Approaches and Methods to Measure Oxidative Stress in Clinical Samples: Research Applications in the Cancer Field. *Oxidative Medicine and Cellular Longevity*, *2019*, 1–29. https://doi.org/10.1155/2019/1279250

86. da Silva, R. C., Eleftheriou, K., Recchia, D. C., Portegijs, V., ten Bulte, D., Kupfer, N., Vroegindeweij-de Wagenaar, N. P., Vergara, X., Ouchene, A., van den Heuvel, S., & Baubec, T. (2025). Engineered chromatin readers track damaged chromatin dynamics in live cells and animals. *Nature Communications*, *16*(1). https://doi.org/10.1038/s41467-025-65706-y

87. Basu, S., Campbell, H. M., Dittel, B. N., & Ray, A. (2010). Purification of Specific Cell Population by Fluorescence Activated Cell Sorting (FACS). *Journal of Visualized Experiments*, *41*. https://doi.org/10.3791/1546